IEEE Access
Multidisciplinary ⋮ Rapid Review ⋮ Open Access Journal

Received 9 February 2023, accepted 19 February 2023, date of publication 27 February 2023, date of current version 8 March 2023.

Digital Object Identifier 10.1109/ACCESS.2023.3249295

RESEARCH ARTICLE

Finite-Time Integral Backstepping Nonsingular Terminal Sliding Mode Control to Synchronize a New Six-Term Chaotic System and Its Circuit Implementation

NAPASOOL WONGVANICH[1], (Member, IEEE), NATCHANAI ROONGMUANPHA[2], AND WORAPONG TANGSRIRAT[1]

[1]Department of Instrumentation and Control Engineering, School of Engineering, King Mongkut's Institute of Technology Ladkrabang, Bangkok 10520, Thailand
[2]KOSEN-KMITL, King Mongkut's Institute of Technology Ladkrabang, Bangkok 10520, Thailand

Corresponding author: Worapong Tangsrirat (worapong.ta@kmitl.ac.th)

This work was supported by King Mongkut's Institute of Technology Ladkrabang under Grant 2566-02-01-009.

ABSTRACT This work presents the finite-time synchronization of a new six-term chaotic system with only stable equilibria and its circuitry implementation. The chaotic system is designed in such a way that its complex dynamical behavior, including hidden attractors, can be adjusted through only one parameter, whilst allowing transformation to chaotic flows via invariant transformations. A finite-time chaotic synchronizer is designed via a nonsingular terminal integral backstepping sliding mode controller, with reduced theoretical finite-time convergence, and a modified sliding surface, to accommodate analog circuitry implementations. A comparison between the proposed controller against conventional integral backstepping sliding mode controller showed that active synchronization is achieved in finite time. Finally, analog circuitry implementation for both open-loop and closed-loop configurations is realized via commercially available active components such as LF357 and AD633. The descriptive circuitry equations for both configurations are designed to mimic the actual governing control equations for simplicity and ease of circuit troubleshooting. The workability of both configurations was tested in OrCAD PSpice. Results show that the master and slave systems were found to be in synchronization with less than 0.95% maximum errors.

INDEX TERMS Chaotic system, attractor, chaos synchronization, finite-time integral backstepping control, terminal sliding mode control, closed-loop circuit implementation.

I. INTRODUCTION

Chaos theory, since its conception with the discovery of the well-known Lorenz system [1], has gradually blossomed over the years. Its essence lies in the description of the apparently simple, well-behaved systems of differential equations. Well-known essential characteristics of chaotic systems include sensitivity to initial conditions, as well as the existence of the infinite number of periodic responses [2], whose characteristics also include long-term unpredictability [3]. Many chaotic systems have arisen from natural phenomena, namely, atmospheric convection [1], chemical reaction [4], electronic circuits [5]. Since then, the search and design for chaotic systems have been unrelentless. Sprott [6] explored several third-order chaotic systems and classified the systems into two categories: five-term systems with two equilibriums (Sprott A-E), and six terms systems with one equilibrium (Sprott F-S). Other types of 3D chaotic systems that have been designed include, for example, [7], [8], [9], [10], [11], and [12]. The search for chaotic attractors continue with the works of [13], [14], and [15], for some examples.

In the search for chaotic attractors, researchers have also uncovered those with hidden attractions. The first chaotic attractor exhibiting this phenomenon arose from the

The associate editor coordinating the review of this manuscript and approving it for publication was Shihong Ding.

generalized Chua's system [16], leading to the classification of attractors as self-excited or hidden [17]. A self-excited attractor is one whose basin of attraction intersects with an open neighborhood of equilibrium, otherwise, the attractor is *hidden*. Identification of such attractors is important for many engineering applications, as a sudden shift to the undesirable attractor could lead to catastrophes [18], [19]. There have been a number of algorithms that cater to the need for hidden attractor localization. The earliest algorithm was developed by Kuznetsov [16]. An improvement of the Kuznetsov algorithm then compared the Lyapunov spectrum for each trajectory orbit to classify the attractors [20]. This particular algorithm requires an accurate and precise computation of the Lyapunov spectrum, incurring more computational costs. The latest algorithm was developed by Datseris and Wegemakers in 2022 [21] using the Poincare recurrence theorem. A great number of chaotic attractors with hidden attraction phenomena have been unveiled. Some examples include [9], [22], [23].

Although multiple wing systems have been designed in the literature, these generally incur no equilibrium [14], [24], [25]. Attempts at designing multi-wings systems with only stable equilibria are rare in the literature. This is because the design of systems with only stable equilibria is a challenging task in itself. Once a system with stable equilibria is designed, its initial conditions near the equilibrium generally converge to that particular equilibrium, which may not coin the multiple wings if common methods such as the addition of equilibria to the saddle-foci system are simply used. However, designs such as [26] and [27] applied the sigmoid functions in an attempt to generate multiple scroll/wing systems. The latest designs include the use of invariant transformations [28], [29]. Following such design, this paper thus concentrates on devising a chaotic system with only stable equilibria that also contain hidden attractors, and through an invariant transformation, shows that transformations to other multi-wing chaotic systems with only stable equilibria could also be devised.

Synchronization of chaos is the process of oscillating two separate chaotic systems such that their respective trajectories are concurrent. To this end, a control algorithm is needed, as initially there will be synchronization errors whose dynamics arise from the mismatch between the drive and response systems. Various control algorithms have been proposed in the literature including linear feedback control [30], [31], adaptive control [32], [33], [34], [35], optimal control [36], [37], and nonlinear control [38], [39], [40], [41], [42], [43]. Adaptive backstepping control was used in [44], [45], [46], and [47]. Vaseghi et al. [48] employed adaptive sliding mode control for secure communication in wireless sensor networks, demonstrating of the robustness of the closed-loop system. Traditional integral sliding mode controller appends the integral action to the system state variables, readily eliminating steady-state errors as well as improving the robustness [49]. However, like its traditional integral action in a PID controller, the windup effect causes a large overshoot or a longer transition time in the control. To generate a finite time transition, it is then necessary to select a sufficiently large sliding mode surface. However, such a move invariably leads to instability and introduces the well-known chattering phenomenon, which degrades the actuator through wear and tear [50]. In this light, nonsingular fast terminal sliding mode control was proposed to achieve the chattering alleviation feature [51]. Other works then proposed the global terminal backstepping control technology [52], [53], as well as nonsingular integral type control laws [54], [55]. Based on the survey of the literature, it is then paramount that the controller be designed for the chaos synchronization needed to achieve such synchronization in finite time. Although the chattering-free feature is not quite as important as the closed-loop finite-time response since our application does not involve a motor as the actuator for the system, it is still indeed desirable. Most importantly, the designed controller must be able to be implemented using analog circuitry. This closed-loop implementation has never been done before in any literature since researchers thus far have only been concerned with the open-loop circuit implementation of chaotic systems.

In summary, this work thus originates the following key contributions:

1) The conjuration of a six-term chaotic system with only stable equilibria, capable of being transformed into other multi-wing chaotic systems via invariant transformation, whose complex dynamics could be changed with only one parameter.
2) The design of a nonlinear, nonsingular integral backstepping terminal sliding mode control for synchronization of the designed six-term chaotic system. Furthermore, a theoretical proof is provided that provides faster reaching time T_{reach} than earlier works of [56] and [57], allowing finite-time control.
3) The practical implementation of both open-loop and closed-loop systems using analog circuitry through commercially available active components such as LF357 and AD633.

The paper is now organized as follows: Section II outlines the presented six terms chaotic system, along with its dynamical analyses and transformation to other chaotic systems. Section III then designs the open loop system, along with its implementation using analog circuitry. Section IV designs a nonlinear, nonsingular finite-time integral backstepping terminal sliding mode control for synchronization of the designed six-term chaotic system, with its circuit implementation conducted in Section V. Section VI then draws the conclusion of this work.

II. THE PRESENTED SIX-TERM CHAOTIC SYSTEM

In this section, we first present the novel six-term chaotic system with two equilibria, whose stability nature can be made stable or unstable depending on the value of the lone system parameter. Detailed dynamical system analysis including bifurcation and hidden chaotic attraction are also analyzed.

A. MATHEMATICAL MODEL AND BASIC PROPERTY OF THE SYSTEM

Inspired by the addition of the ax feedback term to the original Sprott-B system in [29], we add the same term to the first equation of the original Sprott-C system [6]. The resulting equations of motion are:

$$\begin{aligned}\dot{x}_1 &= ax_1 + x_2x_3\\ \dot{x}_2 &= x_1 - x_2\\ \dot{x}_3 &= 1 - x_1^2\end{aligned} \tag{1}$$

where parameter a is the system parameter. Note that the original Sprott-C system is the case of a being zero. This system, being similar to the Sprott-B system, is also invariant under the transformation $(x_1, x_2, x_3) \rightarrow (-x_1, -x_2, x_3)$. This means that the presented system will be symmetric about the x_3 axis and has rotation symmetry for x_3.

1) EQUILIBRIA

Setting the right-hand side of Equation (1) to zero and solving, two equilibrium points are easily found to be:

$$E_1 = [1, 1, -a]^T \tag{2}$$

$$E_2 = [-1, -1, -a]^T. \tag{3}$$

We are next interested in the local stability of the equilibrium points E_1 and E_2. This is provided simply through the linearization of the system. Evaluating the jacobian at the equilibrium point E_1 gives:

$$J_{E_1} = \begin{bmatrix} a & -a & -1 \\ 1 & -1 & 0 \\ 2 & 0 & 0 \end{bmatrix}. \tag{4}$$

The characteristic polynomial of J_{E_1} is:

$$s^3 + (1 - a)s^2 + 2\,s + 2. \tag{5}$$

To ensure that the roots of this characteristic polynomial have negative real parts, we require the condition of $1 - a > 0$; that is, $a < 1$. Evaluating the jacobian at the equilibrium E_2 gives:

$$J_{E_2} = \begin{bmatrix} a & -a & 1 \\ 1 & -1 & 0 \\ -2 & 0 & 0 \end{bmatrix}. \tag{6}$$

In this case, the characteristic polynomial is

$$s^3 + (1 - a)s^2 + 2\,s + 2.$$

Note that this characteristic polynomial is identical to the one computed in Equation (5). This is because our system has symmetry embedded in it, as evidenced clearly by the computed jacobians J_{E_1} and J_{E_2}. We can thus conclude that the system will indeed be locally stable for all $a < 0$. Note also that the presented system has no amplitude parameter due to being dependent on only a single parameter a. However, what it does offer is the existence of multiple locally stable equilibria, which greatly simplifies the dynamical systems analysis. This feature in itself is challenging from the chaotic systems point of view [29].

2) DISSIPATIVITY

For the dynamical system given by Equation (1), the dissipativity of the system is given by the trace of the jacobian J_{E_1} and J_{E_2}:

$$\begin{aligned}\nabla V &= \frac{\partial \dot{x}_1}{\partial x_1} + \frac{\partial \dot{x}_2}{\partial x_2} + \frac{\partial \dot{x}_3}{\partial x_3} = \text{Trace}\left(J_{E_1}\right) = \text{Trace}\left(J_{E_2}\right)\\ &= a - 1\end{aligned} \tag{7}$$

The divergence value is less than one for all $a < 1$. So the exponential contraction rate for the flows of Equation (1) is given by:

$$\frac{dV}{dt} = -(1 - a)V \tag{8}$$

Hence an initial volume V_0 will shrink according to $V(t) = V_0 e^{-(1-a)t}$. This means that as the system is locally stable, the flow shrinks to zero. Note that this system does not have a global attractor that is able to trap all the solution trajectories into a bounded region according to the definition of [58]. However, with special initial conditions, potential local attractors may still exist. These attractors will be uncovered with a more dynamic system analysis in the next section.

B. DYNAMICAL ANALYSIS

In this section, we give the dynamic system analysis of the presented system. The numerical simulations are mainly carried out using the differential equation solver `ode45` in MATLAB, and the `DynamicalSystems` package in Julia software [59].

1) LYAPUNOV EXPONENTS

The Lyapunov exponent is one of the most important means for probing a dynamical system for chaotic activity, characterizing the deviation of infinitesimally close trajectories by giving an average exponential rating. A positive maximum Lyapunov exponent is indicative of chaotic behavior [60]. For numerical investigation of the finite time Lyapunov exponents of the presented system, we use the adaptive time step, with the simulation time of 20000 seconds [61], [62]. When the parameter a is set at $a = -0.042$, with initial conditions of $\mathbf{x}_0 = [4, 1, 1]^T$, the Lyapunov spectrum computed from the algorithm of Wolf [63] is:

$$L_1 = 0.116,\ L_2 = 0,\ L_3 = -1.158. \tag{9}$$

This particular set of initial conditions and parameter a indeed generate flows with expanding nature in phase space. Hence, the proposed system is indeed chaotic. The Lyapunov dimension is computed to be:

$$D = 1 - \frac{L_1}{L_3} = 1 - \frac{0.116}{-1.158} = 1.100 \tag{10}$$

The other popular fractal dimension used to quantify chaos is the Kaplan-Yorke dimension, which is calculated from the Lyapunov exponents using the following formula:

$$D_{KY} = k + \frac{\sum_{i=1}^{k} L_i}{|L_{k+1}|} \tag{11}$$

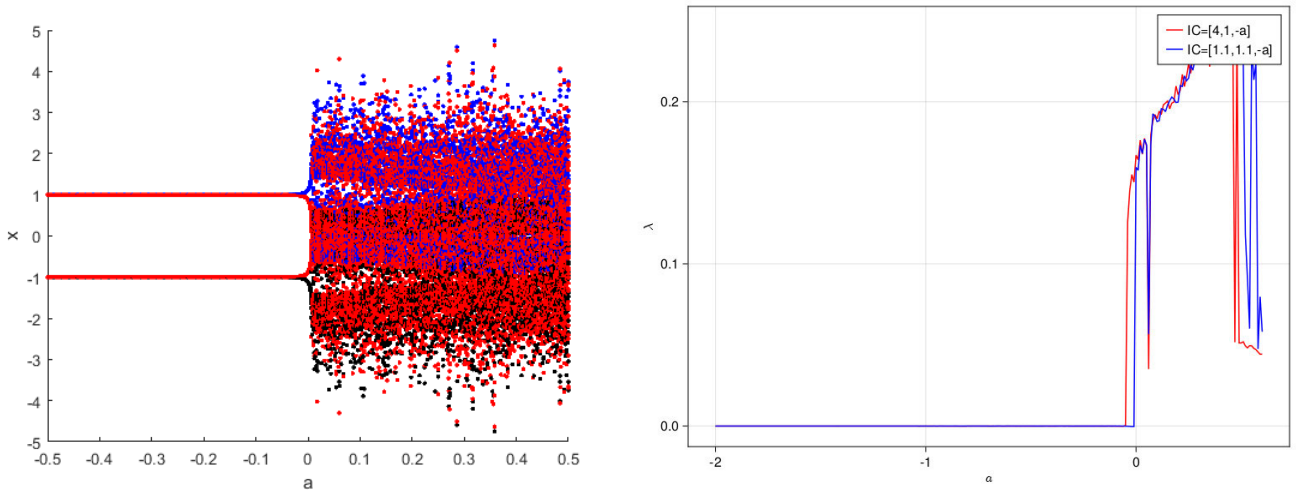

(a) Bifurcation diagram for the maxima and minima of state x_1.

(b) Corresponding maximum Lyapunov exponent for two initial conditions

FIGURE 1. **Bifurcation diagrams with respect to the states and maximum Lyapunov exponent (MLE).**

where k is the smallest integer such that the sum of all the Lyapunov exponents are non-negative so that chaotic trajectory is guaranteed. In our case, $k = 2$, which implies that

$$D_{KY} = 2 + \frac{L_1 + L_2}{|L_3|} = 2 + \frac{0.116}{1.158} = 2.100$$

2) BIFURCATION

The bifurcation diagram is an important tool in the study of dynamical systems in general, as it depicts the relationship between a parameter of the system and the behavior of the dynamical system in which the parameter in question is measured. For the varying parameter a, Fig. 1 shows the bifurcation diagram for the maxima and minima of the state x_1 against the change in the parameter $a \in [-0.5, 0.5]$, where the blue, black and red plots are the orbits generated by the initial conditions $[1.1, 1.1, -a]^T$, $[-1.1, -1.1, -a]^T$, $[4, 1.1, -a]^T$, respectively. As is seen, for values of a less than zero roughly, the initial conditions $[1.1, 1.1, -a]^T$ (blue) and $[-1.1, -1.1, -a]^T$ (black) generate orbits that are eventually attracted to the stable equilibrium points. The initial condition $[4, 1.1, -a]^T$ (red), on the other hand, generates a multi-stable orbit about both equilibrium points. As parameter a becomes positive, all initial conditions generate chaotic orbits. Note that both equilibria are locally stable for all parameters ranges used in the bifurcation analysis, but the system in Equation (1) can still exhibit stable dense orbit with positive Lyapunov exponent as was seen in the earlier discussion. This implies that the system is chaotic with stable equilibria. Fig. 1b shows the corresponding bifurcation diagram of the maximum Lyaponov exponents for the initial conditions $[1.1, 1.1, -a]^T$ (blue) and the $[4, 1.1, -a]^T$ (red). It is seen that for $a < -0.042$, the maximum Lyaponov exponent is zero, signifying the occurrence of stable limit cycles for both sets of initial conditions. As a increases over -0.042, the initial conditions $[4, 1.1, -a]^T$ suddenly generate chaotic flows, while the initial conditions $[1.1, 1.1, -a]^T$ still generate stable limit cycle flows. This fact implies that coexisting bifurcation routes could be generated by different initial conditions, indicating possible hidden attractors.

To see the effect of Fig.1b even more clearly, Fig.2a and Fig.2b plot the phase portrait of the system of Equation (1) for $a = -0.042$ with the initial conditions $[1.1, 1.1, -a]^T$ and $[4, 1.1, -a]^T$, respectively. It is clearly seen that the flows from the initial conditions $[1.1, 1.1, -a]^T$ converge to the equilibrium E_1, while the flows from the initial conditions $[1.1, 1.1, -a]^T$ form a double-wing chaotic attractor. It can be conjectured that had we used the initial conditions $[-1.1, -1.1, -a]^T$, the orbit coined from these particular initial conditions would have converged to the second equilibrium E_2.

3) BASIN OF ATTRACTION

The existence of coexisting bifurcation routes to different initial conditions with the same parameter prompts us to further investigate the combinations of initial conditions that would end up converging to either equilibrium E_1 and E_2, or else end up with chaotic flows. Since both equilibria have a common x_3, that is, $x_3 = -a$, a basin of attraction plot can be computed for the case of $a = -0.042$, which is shown in Fig.3. The orange basin shows all the initial conditions combinations converging to the equilibrium E_1, while the white basin shows the set of initial conditions converging to the equilibrium E_2. The blue basin shows the initial conditions converging to the chaotic flows. The Poincare map with the cut at $z(0) = -a$ is also shown in yellow on the basin of the attraction plot. It is seen that the Poincare map does not intersect the equilibria E_1 and E_2, thereby revealing the

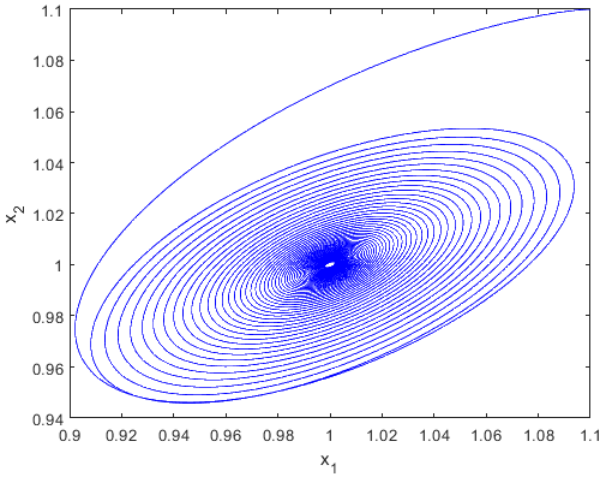

(a) Phase portrait for $[x_1, x_2]$ for initial condition $[1.1, 1.1, -a]^T$

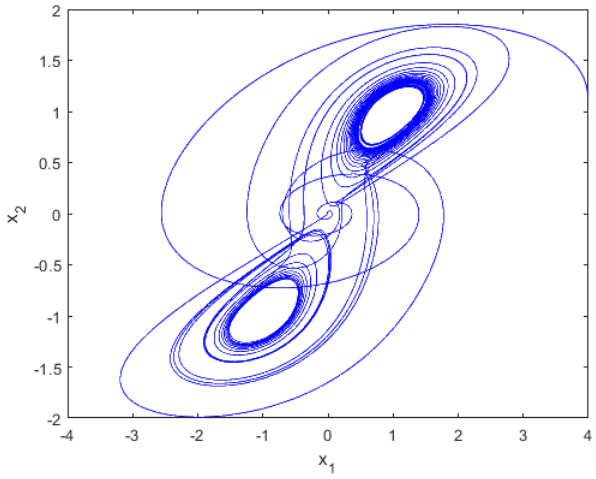

(b) Phase portrait for $[x_1, x_2]$ for initial condition $[4, 1.1, -a]^T$

FIGURE 2. Phase portraits of system (1) with different initial conditions.

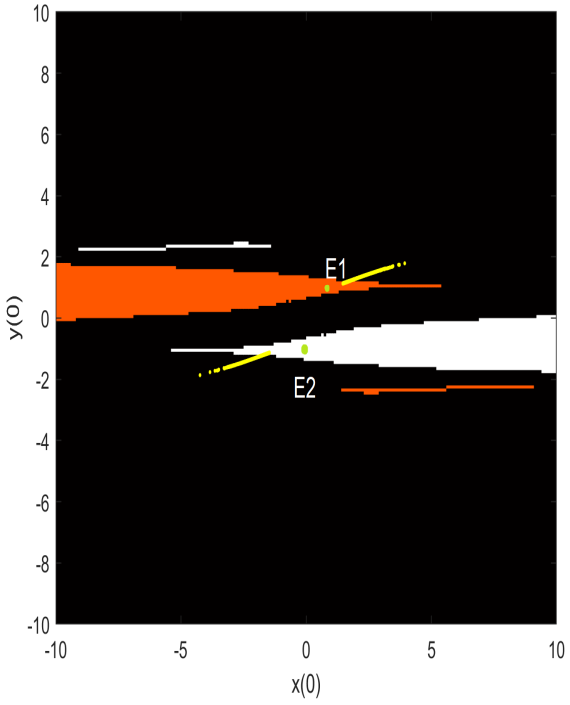

FIGURE 3. Basin of attraction for the chaotic attractor for a=-0.042 and $x_3(0) = -a$.

existence of the hidden attractors for the chaotic system given by Equation (1).

C. TRANSFORMATION TO OTHER CHAOTIC FLOWS THROUGH SYMMETRY

As noted in Section II-A that the presented system has embedded rotation symmetry about the x_3 axis. It is thus possible to create other chaotic flows by invariant rotation action $C_n = R_n(\frac{2\pi}{3})$ about the x_3 axis [28], [29]. In other words, the imaging system may be obtained by a $2 \to 1$ mapping $\Phi_n := R^3(x_1, x_2, x_3) \to R^3(\tilde{x}_1, \tilde{x}_2, \tilde{x}_3)$ defined [28], [29]:

$$\begin{aligned} \tilde{x}_1 &= \mathrm{Re}(x_1 + jx_2)^2 = x_1^2 - x_2^2 \\ \tilde{x}_2 &= \mathrm{Im}(x_1 + jx_2)^2 = 2\, x_1 x_2 \\ \tilde{x}_3 &= x_3 \end{aligned} \tag{12}$$

To obtain the mapped system, we simply rewrite the original system of Equation (1) with the tilde notation:

$$\begin{aligned} \dot{\tilde{x}}_1 &= a\tilde{x}_1 + \tilde{x}_2\tilde{x}_3 \\ \dot{\tilde{x}}_2 &= \tilde{x}_1 - \tilde{x}_2 \\ \dot{\tilde{x}}_3 &= 1 - \tilde{x}_1^2 \end{aligned} \tag{13}$$

Carrying out the required differentiation of Equation (12), equating it to Equation (13), and solving for x_1 and x_2, the mapped system is thus:

$$\begin{aligned} \dot{x}_1 &= \frac{ax_1(x_1^2 - x_2^2) + x_2(-2x_1x_2 - x_2^2 + x_1^2(1 + 2\, x_3))}{2(x_1^2 + x_2^2)} \\ \dot{x}_2 &= \frac{x_1^3 - (2 + a)x_1^2x_2 + ax_2^3 - x_1x_2^2(1 + 2\, x_3)}{2(x_1^2 + x_2^2)} \\ \dot{x}_3 &= 1 - (x_1^2 - x_2^2)^2. \end{aligned} \tag{14}$$

The equilibria of the transformed system is:

$$E_1 = \left[-\sqrt{\frac{1}{\sqrt{2}} - \frac{1}{2}}, \sqrt{\frac{1}{2} + \frac{1}{\sqrt{2}}}, -a \right]^T, \tag{15}$$

$$E_2 = \left[\sqrt{\frac{1}{\sqrt{2}} - \frac{1}{2}}, -\sqrt{\frac{1}{2} + \frac{1}{\sqrt{2}}}, -a \right]^T, \tag{16}$$

$$E_3 = \left[-\sqrt{\frac{1}{2} + \frac{1}{\sqrt{2}}}, -\sqrt{\frac{1}{\sqrt{2}} - \frac{1}{2}}, -a \right]^T, \tag{17}$$

$$E_4 = \left[\sqrt{\frac{1}{2} + \frac{1}{\sqrt{2}}}, \sqrt{\frac{1}{\sqrt{2}} - \frac{1}{2}}, -a \right]^T. \tag{18}$$

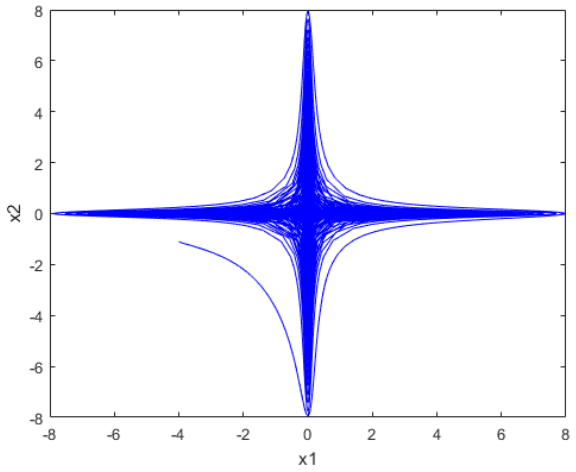

(a) Phase portrait for $[x_1, x_2]$ for initial condition $[4, 1.1, -a]^T$ for the transformed system

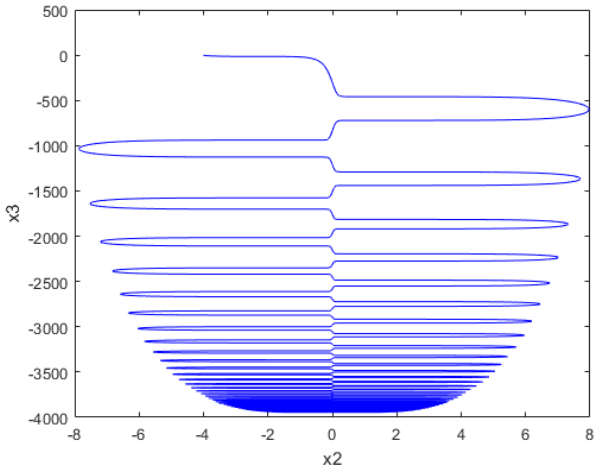

(b) Phase portrait for $[x_1, x_2]$ for initial condition $[4, 1.1, -a]^T$ for the transformed system

FIGURE 4. Phase portraits for the transformed system described by Equation (14).

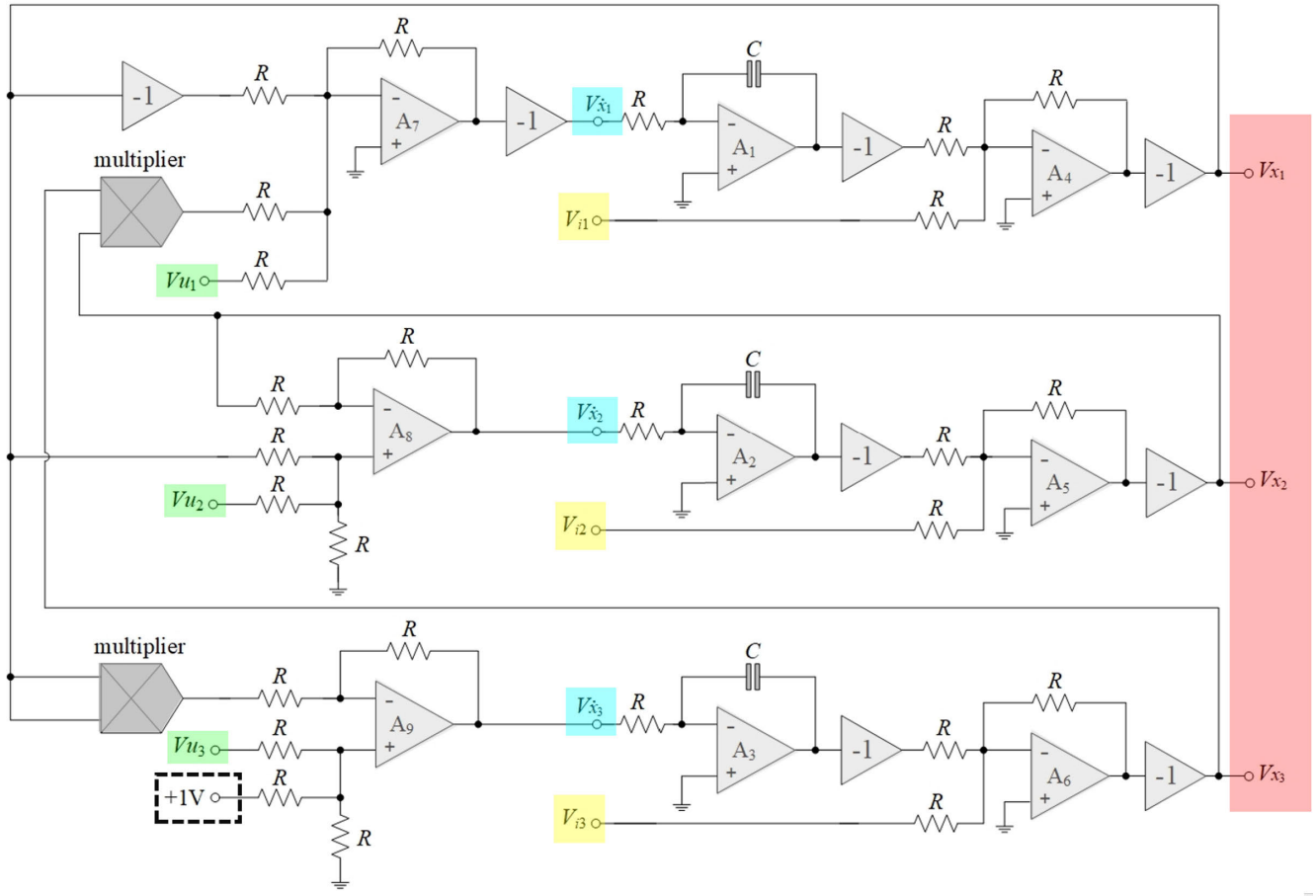

FIGURE 5. Overall schematic for the circuit implementation of the presented six-term chaotic open-loop system.

Note that we now have four equilibria instead of two. Fig. 4 plots the phase responses in (x_1, x_2) plane. It is obvious that we now have four wings instead of the two that we previously had, as was shown in Fig. 2b. Since this work is devoted to the study of the system of Equation (1), we leave the full dynamical analysis of the system described by Equation (14) for future work.

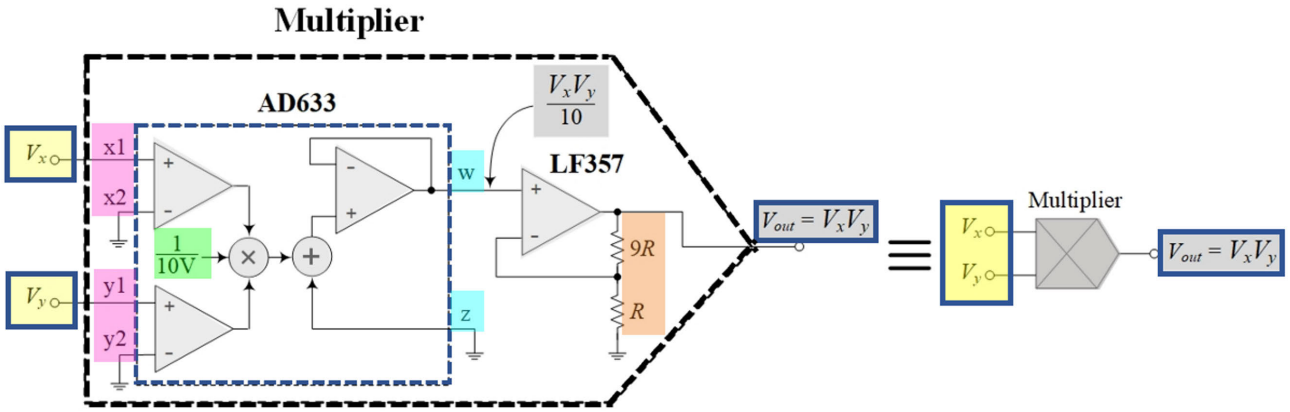

FIGURE 6. Practical circuit implementation of the signal multiplication given by AD633 and LF357.

III. CIRCUIT IMPLEMENTATION OF THE OPEN LOOP SYSTEM

A. CIRCUIT DESIGN METHODOLOGY

The open-loop model of Equation (1) admits a corresponding circuit implementation as depicted in Fig. 5. The overall circuit topology is an operational amplifier (OA) based design, with three integrators (A_1-A_3), four summers (A_4-A_7), two differential amplifiers (A_8, A_9), eight signal inverters and two multipliers. Analysis of the proposed circuit schematics yields the following system of differential equations:

$$\begin{aligned} V_{\dot{x}_1} &= aV_{x_1} + V_{x_2}V_{x_3} \\ V_{\dot{x}_2} &= V_{x_1} - V_{x_2} \\ V_{\dot{x}_3} &= 1 - V_{x_1}^2 \end{aligned} \tag{19}$$

$$a = \frac{R_1}{R} \tag{20}$$

Note that this circuit formulation given by Equation (19) has the exact same form as the original system given by Equation (1), where the variable $V_{xk}, k = 1, 2, 3$ denotes the voltage of state x_k. Note also from Equation (20) that the value of the system parameter a can be adjusted simply by choosing an appropriate value of resistor R_1. The initial conditions for the open-loop chaotic system are set electronically by directly adjusting the reference applied voltage through the V_{x_k} terminal.

B. PSPICE SIMULATION

To prove the design concept, the modified Sprott-C chaotic open-loop system in Fig.5 was simulated with commercially available integrated circuits (ICs) using OrCAD PSPICE simulation program. The op-amps used were taken from the commercially available macro-model of OA LF357 by National Semiconductor [64], as well as analog multiplier AD633 by Analog Devices [65]. Both types of device were biased with symmetrical supply voltages of ±5 V. According to Fig.6, the signal multiplier section in Fig.5 was realized by cascading the connections of an analog multiplier AD633 and a non-inverting amplifier LF357. The component values were set at $R_1 = 420\,\Omega$, $R = 10\,k\,\Omega$, $C = 100\mu$F.

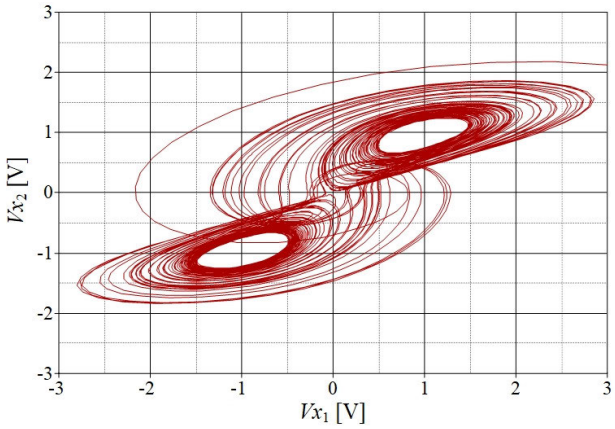

FIGURE 7. Phase portrait for the circuit simulation of the open-loop system for the initial condition $[5, 1.1, -a]^T$.

All of the input channels V_{uk} were also kept grounded (i.e. $V_{uk} = 0$ V). The initial conditions of the proposed system were simply set through the applied voltages V_{i1}, V_{i2} and V_{i3} of the circuit shown in Fig.5, where the system parameter a (−0.042) must match the magnitude value of v_{i3}. Fig. 7 shows the phase portrait for the circuit implementation of the open-loop system for $[V_{x_1}, V_{x_2}]$ plane for the initial condition $[5, 1.1, 0.042]^T$, demonstrating the double wing chaotic attractor, as expected from the basin of attraction in Fig. 3.

IV. FINITE TIME INTEGRAL BACKSTEPPING SLIDING MODE SYNCHRONIZATION OF THE CHAOTIC SYSTEM

In this section, we present the design of the finite-time integral backstepping nonsingular terminal sliding mode control for the synchronization of the presented 3D chaotic system.

A. CONTROL PROBLEM FORMULATION AND PRELIMINARIES

1) CHAOS CONTROL PROBLEM FORMULATION

We first note, however, that there are two types of control problems of interest in the study of chaotic systems: active

stabilization and synchronization. We demonstrate, with mathematical proof, that in terms of the error dynamics, the two problems end up being identical.

In the active stabilization problem, the main goal is to design a controller to drive all the states x_1, x_2, x_3 to zero, so that all chaos disappears [66]. In an active synchronization problem, the main control goal is to drive a chaotic system, called the slave system, to be in sync with an original chaotic system which is termed the master system [67]. For the presented system of this work, the master system is the original system in Equation (1), repeated here for convenience:

$$\begin{aligned}\dot{x}_{m,1} &= a x_{m,1} + x_{m,2} x_{m,3} \\ \dot{x}_{m,1} &= x_{m,1} - x_{m,2} \\ \dot{x}_{m,1} &= 1 - x_{m,1}^2 \end{aligned} \tag{21}$$

The slave system is equipped with the controller to be designed, and is thereby written:

$$\begin{aligned}\dot{x}_{s,1} &= a x_{s,1} + x_{s,2} x_{s,3} + u_1 \\ \dot{x}_{s,2} &= x_{s,1} - x_{s,2} + u_2 \\ \dot{x}_{s,3} &= 1 - x_{s,1}^2 + u_3 \end{aligned} \tag{22}$$

Theorem 1: The error dynamics of the active stabilization problem are equivalent to the active synchronization problem and are given by:

$$\begin{aligned}\dot{e}_1 &= e_2, \\ \dot{e}_2 &= e_3, \\ \dot{e}_3 &= v. \end{aligned} \tag{23}$$

Proof: The active stabilization problem can be viewed, in terms of Equation (22), as driving the slave system to zero states. The error states are given simply as the original states themselves i.e. $e_1 = x_{s,1}$, $e_2 = x_{s,2}$, and $e_3 = x_{s,3}$. Designing the transformative control in terms of the error states as:

$$u_1 = -a e_1 - e_2 e_3 + e_2 \tag{24}$$

$$u_2 = -e_1 + e_2 + e_3 \tag{25}$$

$$u_3 = e_1^2 - 1 + v \tag{26}$$

It is obvious that system (22) has now transformed into the system (23).

For the active synchronization problem, define the error states as $e_i = x_{s,i} - x_{m,i}$, $i = 1, 2, 3$. The error dynamics are given by:

$$\begin{aligned}\dot{e}_1 &= a e_1 + x_{s,2} x_{s,3} - x_{m,2} x_{m,3} + u_1 \\ \dot{e}_2 &= e_1 - e_2 + u_2 \\ \dot{e}_3 &= x_{m,1}^2 - x_{s,1}^2 + u_3 \end{aligned} \tag{27}$$

Designing the transformative control as;

$$u_1 = -a e_1 - x_{s,2} x_{s,3} + x_{m,2} x_{m,3} + e_2, \tag{28}$$

$$u_2 = e_2 - e_1 + e_3, \tag{29}$$

$$u_3 = x_{s,1}^2 - x_{m,1}^2 + v. \tag{30}$$

It is again obvious that the error dynamics of the active synchronization problem is again given by the system of Equation (23). These error dynamics are equivalent to the active stabilization problem. ■

2) PRELIMINARIES

We present in this section the general control problem formulation, where some lemmas and theorems relating to the control design strategy are outlined and presented.

Consider the following general class of nonlinear SISO system written in state space as [68]:

$$\begin{aligned}\dot{x}_1 &= f_1(\bar{x}_1) + g_1(\bar{x}_1) x_2 \\ \dot{x}_2 &= f_2(\bar{x}_2) + g_2(\bar{x}_2) x_3 \\ &\vdots \\ \dot{x}_n &= f_n(x) + g_n(x) u \end{aligned} \tag{31}$$

where $x = [x_1, x_2, \ldots, x_n]^T \in \mathbf{R}^n$ is the state vector with initial condition $x_n(0) = x_0$, $\bar{x}_i = [x_1, x_2, \ldots, x_i]^T$ and $u(t)$ is the control input signal. The functions f_i and g_i $i = 1, \ldots n$ are assumed to be known and Lipschitz on $\Omega_d \subset \mathbf{R}^n$. The control goal is to drive the state x from some arbitrary initial condition to a desired state x_d in finite time.

Lemma 1: [69] If $x_k \in R$ $(k = 1, \ldots, n)$ and $0 < p < 1$, then:

$$\left(\sum_{k=1}^{n} x_k\right)^p \leq \sum_{k=1}^{n} |x_k|^p \leq n^{1-p} \left(\sum_{k=1}^{n} x_k\right)^p$$

Lemma 2: [70] Suppose there exists a $V(x)$ being C^1 smooth positive definite function. The origin $x = 0$ of the nonlinear system (31) will be a finite time stable equilibrium if the following inequality is satisfied for some $\alpha > 0$, $\gamma \in (0, 1)$

$$\dot{V}(x) \leq -\alpha V^{\gamma} \tag{32}$$

The reach time is given by:

$$T_{reach} = \frac{V(0)^{1-\gamma}}{\alpha(1-\gamma)} \tag{33}$$

Proof: We simply solve Equation (32) using the ordinary method of separating variables and integrating from 0 to t. Hence:

$$\begin{aligned} V^{-\gamma} \frac{dV}{dt} &\leq -\alpha \\ \int_0^t \frac{dV}{V^{\gamma}} &\leq -\int_0^t \alpha \, dt \\ \frac{V^{1-\gamma}(t)}{1-\gamma} &\leq \frac{V(0)^{1-\gamma}}{1-\gamma} - \alpha t \\ \implies V(t) &\leq \left[V(0)^{1-\gamma} - \alpha t (1-\gamma)\right]^{\frac{1}{1-\gamma}}. \end{aligned} \tag{34}$$

The time T_{reach} is thus given by the time taken for $V(t) \leq 0$ or:

$$T_{reach} = \frac{V(0)^{1-\gamma}}{\alpha(1-\gamma)}.$$

■

Lemma 3: [56] Consider the nonlinear system (31). Suppose that there exists a C^1 positive definite function $V(x)$

such that the following inequality is satisfied for some scalars $\alpha > 0$, $\gamma \in (0, 1)$ *and* $\rho_1 > 0$*:*

$$\dot{V}(x) \leq -\alpha V^{\gamma} + \rho_1, \tag{35}$$

then the system (32) will be semi-global practical finite time stable (SGPFS).

Proof: The proof of this lemma is easily adapted from the one presented in [56] and [71]. We will suppose that there is a scalar $\theta \in (0, 1)$ enabling the inequality (35) to be rewritten as:

$$\dot{V}(x) \leq -\theta\alpha V^{\gamma} - (1-\theta)\alpha V^{\gamma} + \rho_1$$

Suppose that there exists a state x such that:

$$V^{\gamma} > \frac{\rho_1}{(1-\theta)\alpha},$$

Then the overall inequality (35) is reduced to:

$$\dot{V}(x) \leq -\theta\alpha V^{\gamma}. \tag{36}$$

Invoking the result of Lemma 2, the system will then reach $\{\Omega_x : V^{\alpha}(x) \leq \frac{\rho_1}{(1-\theta)\alpha}\}$ at:

$$T_{reach} = \frac{1}{\theta\alpha(1-\gamma)}\left[V^{1-\gamma}(0) + \left(\frac{\rho_1}{\alpha(1-\theta)}\right)^{\frac{1}{1-\gamma}}\right]. \tag{37}$$

If the system is already at Ω_x, then its trajectory will not exceed the bounds of Ω_x. Hence system (31) will be SGPFS. ■

Lemma 4: [68] Consider the nonlinear system (31). The system will be SGFPS if there exists a C^1 *positive definite function* $V(x)$ *such that the following inequality is satisfied for some scalars* $\alpha_1 > 0$, $\alpha_2 > 0$, $\gamma \in (0, 1)$ *and* $\rho_2 > 0$*:*

$$\dot{V}(x) \leq -\alpha_1 V - \alpha_2 V^{\gamma} + \rho_2. \tag{38}$$

For scalar $\theta_0 \in (0, 1)$*, the reach time is given by [68]:*

$$T_{reach} = \max(T_1, T_2) \tag{39}$$

$$T_1 = t_0 + \frac{1}{\theta_0\alpha_1(1-\gamma)} \ln \frac{\theta_0\alpha_1 V^{1-\gamma}(t_0) + \alpha_2}{\alpha_2}, \tag{40}$$

$$T_2 = t_0 + \frac{1}{\alpha_1(1-\gamma)} \ln \frac{\alpha_1 V^{1-\gamma}(t_0) + \theta_0\alpha_2}{\theta_0\alpha_2} \tag{41}$$

Proof: The proof proceeds in a similar fashion to [68] and Lemma 4 and will be omitted. ■

Remark 1: It follows from Remark 5 in the work of [68] that condition (38) provides a faster convergence rate than inequality (35) when the state is far away from the equilibrium point. Indeed, setting $\alpha_2 = 0$*, the sufficient condition (38) becomes condition* $\dot{V} \leq -\alpha_1 V + \rho_2$*, which is the ordinary control scheme.*

Proposition 1: Consider the nonlinear system (31), a C^1 *positive definite Lyapunov function* $V(x)$*, and the same scalars* $\alpha_1 > 0$, $\alpha_2 > 0$, $\gamma \in (0, 1)$ *and* $\rho_2 > 0$ *of Lemma 4. The following inequality is satisfied*:

$$-\alpha_1 V - \alpha_2 V^{\gamma} + \rho_2 \leq -\min(\alpha_1, \alpha_2) V^{\frac{\gamma+1}{2}} + \varrho \tag{42}$$

where $\varrho = \max(\alpha_1, \alpha_2) + \rho_2$.

Proof: The proof of this proposition is easily verified by direct computation for quadratic and non-quadratic Lyapunov functions. ■

Corollary 1: Consider the nonlinear system (31), an associated positive definite function $V(x)$ *and the scalars* $\alpha_1 > 0$, $\alpha_2 > 0$, $\gamma \in (0, 1)$, $\theta_0 \in (0, 1)$ *and* $\rho_2 > 0$ *satisfying the sufficient condition (38). The revised reach time is given by*:

$$T_{revised} = \max(T_1, T_2, T_3) \tag{43}$$

$$T_1 = \textit{Equation (40)} \tag{44}$$

$$T_2 = \textit{Equation (41)} \tag{45}$$

$$T_3 = \frac{2}{\theta_0\bar{\alpha}(1-\gamma)}\left[V^{1-\gamma}(t_0) + \left(\frac{\varrho}{\bar{\alpha}(1-\theta_0)}\right)^{\frac{2}{1-\gamma}}\right]. \tag{46}$$

where $\bar{\alpha} = \min(\alpha_1, \alpha_2)$ *and* $\varrho = \max(\alpha_1, \alpha_2) + \rho_2$.

Proof: Applying Proposition 1 allows the sufficient condition (38) to be written in the form of the condition (35). Consequently, the reaching time is given in the form of Equation (37), with α replaced by $\bar{\alpha}$ and ρ_1 replaced by ϱ. This reaching time is also provided as a bound, and therefore gets added to the maximum operation of Equation (39). ■

Corollary 2: Consider the nonlinear system (31), an associated positive definite function $V(x)$ *and the scalars* $\alpha_1 > 0$, $\alpha_2 > 0$, $\gamma \in (0, 1)$, $\theta_0 \in (0, 1)$ *and* $\rho_2 > 0$ *satisfying the sufficient condition (38). The residual set of the solution of the system (31) will be given by*:

$$\lim_{t > T_{reach}} V(x) \leq \min\left[\frac{\rho_2}{(1-\theta_0)\alpha_1}, \left(\frac{\rho_2}{(1-\theta_0)\alpha_2}\right)^{\frac{1}{\gamma}}, \left(\frac{\varrho}{\bar{\alpha}(1-\theta_0)}\right)^{\frac{2}{\gamma+1}}\right] \tag{47}$$

where the scalars $\bar{\alpha} = \min(\alpha_1, \alpha_2)$ *and* $\varrho = \max(\alpha_1, \alpha_2) + \rho_2$*, as in Corollary 1.*

Proof: The first two terms inside the minimum operator follow directly from Corollary 1 of [68]. The last term follows from an application of Proposition 1 and the proof of Lemma 3, with γ replaced by $\frac{2}{\gamma+1}$, ρ_1 replaced by ϱ and α replaced by $\bar{\alpha}$. ■

Remark 2: The results of Proposition 1 and Corollaries 8-9 imply that even though condition (38) provides a faster convergence rate than (35), a tighter bound is provided for both T_{reach} *and the residual set* $\lim_{t > T_{reach}} V(x)$*. The given bound still implies that the overall convergence rate is faster than the works of [56], [57], as well as the ordinary control approach* $\dot{V} \leq -\alpha_1 V + \rho_2$.

B. CONTROL DESIGN

The error system given by Equation (23) is in the triangular form, facilitating the use of backstepping-based control design [67]. In this respect, define the errors as follows:

$$z_1 = e_1 \tag{48}$$

$$z_2 = e_2 - \eta_1 \tag{49}$$

$$z_3 = e_3 - \eta_2 \tag{50}$$

where η_1 and η_2 are the virtual controls to be designed. To append integral action, we also define the following:

$$\phi_1 = \int_0^t z_1(t)\,dt, \tag{51}$$

$$\phi_2 = \int_0^t z_2(t)\,dt. \tag{52}$$

Step 1: We stabilize the first equation in system (23). Construct the first Lyapunov function:

$$V_1 = \frac{1}{2}z_1^2 + \frac{1}{2}\zeta_1\phi_1^2 \tag{53}$$

Differentiating V_1 with respect to time along the trajectory of the system (23) gives:

$$\begin{aligned}\dot{V}_1 &= z_1 e_2 + \zeta_1 z_1 \phi_1 \\ &= z_1(z_2 + \eta_1 + \zeta_1\phi_1)\end{aligned} \tag{54}$$

Designing $\eta_1 = -\zeta_1\phi_1 - c_1 z_1$, with $c_1 > 0$, will make $\dot{V}_1 < 0$, under the condition, that we force z_2 to converge to zero in the next stage of the design.

Step 2: In this step we focus on the stabilization of the second equation of the system (23). Construct the second Lyapunov function:

$$V_2 = V_1 + \frac{1}{2}z_2^2 + \frac{1}{2}\zeta_2\phi_2^2 \tag{55}$$

Time differentiating V_2 along the trajectory of the system (23) now yields:

$$\dot{V}_2 = -c_1 z_1^2 + z_2\dot{z}_2 + \zeta_2\phi_2 z_2 \tag{56}$$

$$= -c_1 z_1^2 + z_2(z_3 - \eta_2 - \dot{\eta}_1 + \zeta_2\phi_2) \tag{57}$$

Designing $\eta_2 = -\zeta_2\phi_2 + \dot{\eta}_1 - z_3 - c_2 z_2$, with $c_1 > 0$, will make $\dot{V}_2 = -c_1 z_1^2 - c_2 z_2^2 < 0$, thereby stabilizing the second equation of system (23).

Step 3: This last step focuses on stabilizing the last equation of the system (23), as well as determining the real control input $v(t)$. The terminal sliding mode control framework is integrated in this last step of the controller design to exploit its robustness advantages to modeling errors and disturbances, whilst keeping the control design simple enough so that it is implementable since one of the main goals of this work is to implement the closed-loop control design using analog circuitry. The works of Deng [72] and Xu [73] utilized the $\text{sig}(x)^a$ function in their nonsingular terminal sliding mode control designs. The definition is:

$$\text{sig}(x)^a = |x|^a \text{sign}(x) \tag{58}$$

Although the $\text{sig}(x)^a$ function facilitated finite-time sliding mode control [72], [73], the signum function contained in it is much more difficult to implement through circuitry designs. Another persistent problem with the signum function in sliding mode control is the well-known chattering problem, which is normally alleviated in the literature using the hyperbolic tangent ($\tanh(x)$) function. The hyperbolic tangent ($\tanh(x)$) function itself is an approximation of the signum function with some errors near the sign change point

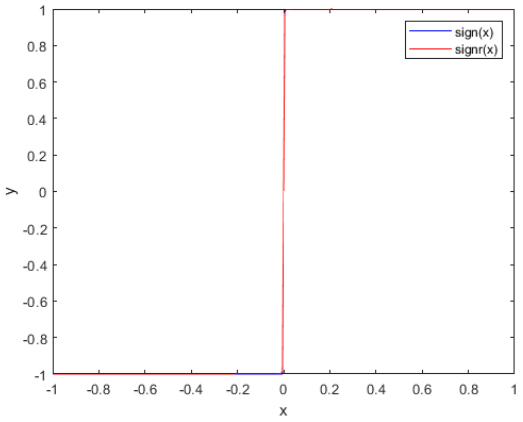

FIGURE 8. The functions sign(x) versus sigr(x).

$x = 0$. With these constraints in mind, we slightly modify the signum function to:

$$\text{signr}(x) = \frac{x}{\sqrt{x^2 + \epsilon^2}}, \quad \epsilon = 0.01. \tag{59}$$

The comparison between the signum function and the signr(x) function is shown in Fig.8, showing close resemblance to one another, with signr(x) being smoother than sign(x) near $x = 0$. The modified $\text{sig}(x)^a$ is thus:

$$\text{sigr}(x)^a = |x|^a \text{signr}(x). \tag{60}$$

Now its derivative is:

$$\frac{d}{dx}\text{sigr}(x)^a = a|x|^{a-1}.$$

Define now the nonsingular terminal sliding surface as:

$$s = z_2 + \frac{a}{\gamma_2 + 1}\text{sigr}(z_3)^{\gamma_2+1}, \quad \gamma_2 \in (0, 1). \tag{61}$$

The time derivative of the sliding surface is simply:

$$\begin{aligned}\dot{s} &= \dot{z}_2 + a|z_3|^{\gamma_2}(v - \dot{\eta}_2), \\ &= e_3 - \dot{\eta}_1 + a|z_3|^{\gamma_2}(v - \dot{\eta}_2).\end{aligned} \tag{62}$$

Note that the control signal comprises two parts in the sliding mode control framework, namely, the equivalent control signal v_c and the switching control signal v_{sw}. The equivalent control signal v_c is designed so that $\dot{s}$ is equal to $-Ds$. Equating Equation (62) to $-Ds$ and solving for the v_c signal yields:

$$v_c = \dot{\eta}_2 + \frac{1}{a}|z_3|^{-\gamma_2}(\dot{\eta}_1 - e_3) - Ds. \tag{63}$$

The switching control signal is designed as:

$$v_{sw} = -D_2\text{sigr}(s)^{\gamma_2}. \tag{64}$$

The total control signal is, thus,

$$\begin{aligned}v &= v_c + v_{sw}, \\ &= \dot{\eta}_2 + \frac{1}{a}|z_3|^{-\gamma_2}(\dot{\eta}_1 - e_3) - Ds - D_2\text{sigr}(s)^{\gamma_2}.\end{aligned} \tag{65}$$

where $D > 0$ and $D_2 > 0$ are chosen in accordance to Lyapunov's stability theory. The parameters γ_2 are chosen to be in the range of (0,1), similar to [72]. The transformative control given by Equations (28) - (30) can now be applied to design the required u_1 - u_3 signals.

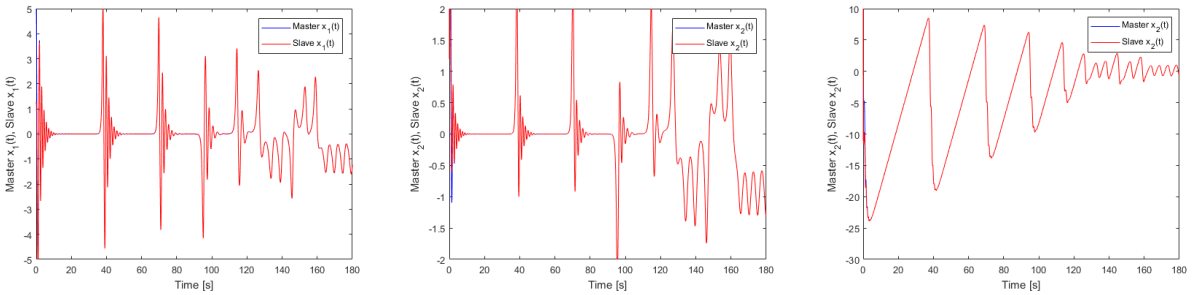

(a) Synchronization of the x_1 state for the master and slave signals

(b) Synchronization of the x_2 state for the master and slave signals

(c) Synchronization of the x_3 state for the master and slave signals

FIGURE 9. Synchronization between master and slave signals.

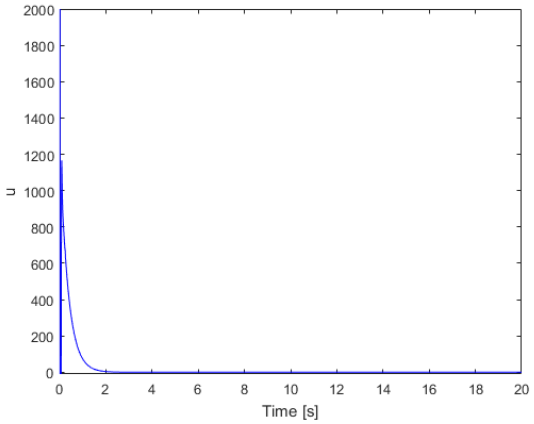

FIGURE 10. The control input $u(t)$ of the chaos synchronization.

C. FINITE TIME STABILITY ANALYSIS

The convergence of the designed controller is now analyzed, including tracking of the desired trajectory x_m.

Theorem 2: Consider the system given by Equation (23), with the control input designed by Equation (65), the system is semi-global practical finite time stable, with the reach time T_{reach} given by:

$$T_{reach} = \max(T_{r_1}, T_{r_2}, T_{r_3}), \tag{66}$$

$$T_{r_1} = \frac{1}{\theta_0 \min(\bar{c}_1, \bar{c}_2)\left(1 - \frac{\gamma_2+1}{2}\right)} \times \ln \frac{\theta_0 \min(\bar{c}_1, \bar{c}_2) V^{1-\frac{\gamma_2+1}{2}}(0) + 2^{1-\frac{\gamma_2+1}{2}} \min(\bar{c}_1, \bar{c}_2)}{2^{1-\frac{\gamma_2+1}{2}} \min(\bar{c}_1, \bar{c}_2)}, \tag{67}$$

$$T_{r_2} = \frac{1}{\min(\bar{c}_1, \bar{c}_2)\left(1 - \frac{\gamma_2+1}{2}\right)} \times = \ln \frac{\min(\bar{c}_1, \bar{c}_2) V^{1-\frac{\gamma_2+1}{2}}(0) + \theta_0 2^{1-\frac{\gamma_2+1}{2}} \min(\bar{c}_1, \bar{c}_2)}{\theta_0 2^{1-\frac{\gamma_2+1}{2}} \min(\bar{c}_1, \bar{c}_2)}, \tag{68}$$

$$T_{r_3} = \frac{2}{\theta_0 \bar{c}\left(1 - \frac{\gamma_2+1}{2}\right)} \times \left[V^{1-\frac{\gamma_2+1}{2}}(0) + \left(\frac{\bar{\nu}}{\bar{c}(1-\theta_0)}\right)^{\frac{2}{1-\frac{\gamma_2+1}{2}}} \right] \tag{69}$$

where $\bar{c}_1 = \min(c_1, c_2, \zeta_1, \zeta_2)$, $\bar{c}_2 = 2^{\frac{\gamma_2+1}{2}} \max(D_1, D_2)$ *and* $\bar{c} = \min\left(\min(\bar{c}_1, \bar{c}_2), 2^{1-\frac{\gamma_2+1}{2}} \min(\bar{c}_1, \bar{c}_2)\right)$, $\bar{\nu} = \max\left(\min(\bar{c}_1, \bar{c}_2), 2^{1-\frac{\gamma_2+1}{2}} \min(\bar{c}_1, \bar{c}_2)\right)$.

Proof: Consider the total Lyapunov function, made up of the integral backstepping control term and the nonsingular terminal sliding mode control term, as follows:

$$V_T = V_1 + V_2 + V_s = V_B + V_s. \tag{70}$$

For the integral backstepping control Lyapunov candidate, we have:

$$\begin{aligned} \dot{V}_B &= -c_1 z_1^2 - c_2 z_2^2 \\ &\leq -c_1 z_1^2 - c_2 z_2^2 - \zeta_1 \phi_1^2 - \zeta_2 \phi_2^2 \\ &\leq -\min(c_1, c_2, \zeta_1, \zeta_2) V_B = -\bar{c}_1 V_B \end{aligned} \tag{71}$$

For the nonsingular terminal sliding mode control, we can write its time derivative as follows:

$$\begin{aligned} \dot{V}_s &= s(-D_1 |s|^{\gamma_2} \text{signr}(s) - D_2 s) \\ &\leq -\max(D_1, D_2) s^2 \\ &\leq -\max(D_1, D_2) 2^{\frac{\gamma_2+1}{2}} V_s^{\frac{\gamma_2+1}{2}} = -\bar{c}_2 V_s^{\frac{\gamma_2+1}{2}}. \end{aligned} \tag{72}$$

Now, seeking an expression of $\dot{V}_T$ in terms of V_T, and using the same coefficients for V_x and $V_x^{\frac{\gamma_2+1}{2}}$, $x \in (B, s)$, we have:

$$\begin{aligned} -\bar{c}_1 V_B - \bar{c}_2 V_s^{\frac{\gamma_2+1}{2}} &\leq -\bar{c}_1 V_B - \bar{c}_2 V_s - \bar{c}_2 V_s^{\frac{\gamma_2+1}{2}} - \bar{c}_1 V_B^{\frac{\gamma_2+1}{2}}, \\ &\leq -\min(\bar{c}_1, \bar{c}_2)(V_B + V_s) \\ &\quad -\min(\bar{c}_1, \bar{c}_2)\left(V_B^{\frac{\gamma_2+1}{2}} + V_s^{\frac{\gamma_2+1}{2}}\right) \end{aligned} \tag{73}$$

Applying Lemma 1 to Equation (73) yields:

$$\begin{aligned} -\bar{c}_1 V_B - \bar{c}_2 V_s^{\frac{\gamma_2+1}{2}} &\leq -\min(\bar{c}_1, \bar{c}_2)(V_B + V_s) \\ &\quad -2^{1-\frac{\gamma_2+1}{2}} \min(\bar{c}_1, \bar{c}_2)(V_B + V_s)^{\frac{\gamma_2+1}{2}}. \end{aligned} \tag{74}$$

Therefore, the total Lyapunov time derivative $\dot{V}_T$ can be expressed as:

$$\dot{V}_T \leq -\min(\bar{c}_1, \bar{c}_2) V_T - 2^{1-\frac{\gamma_2+1}{2}} \min(\bar{c}_1, \bar{c}_2) V_T^{\frac{\gamma_2+1}{2}}. \tag{75}$$

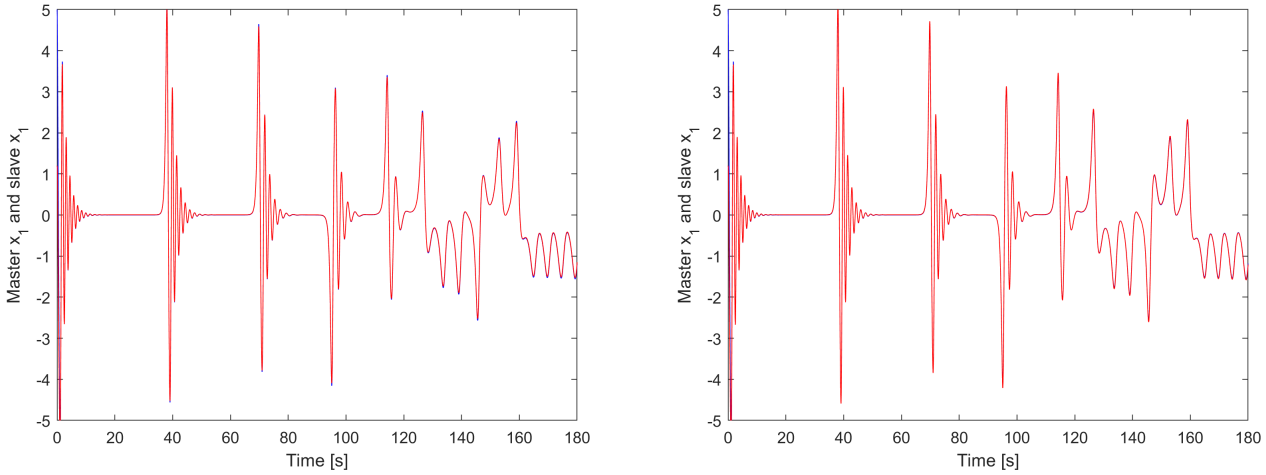

(a) Synchronization of the x_1 state for the master and slave signals when $a = -0.084$

(b) Synchronization of the x_1 state for the master and slave signals when $a = -0.001$

FIGURE 11. Synchronization of the chaotic signals parameter *a* ranging between -0.001 to -0.084.

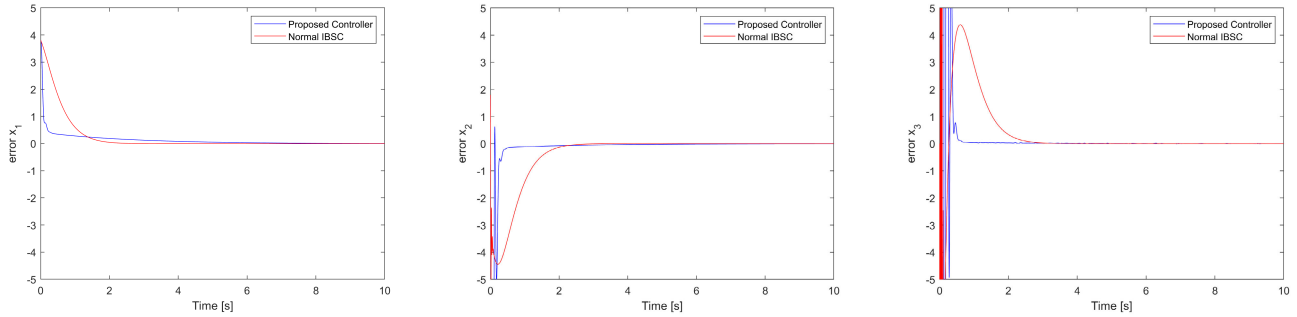

(a) Trajectory comparison of the e_1 state

(b) Trajectory comparison of the e_2 state

(c) Trajectory comparison of the e_3 state

FIGURE 12. Trajectory comparison of the state errors between the proposed finite time IBSMC against the normal IBSMC.

Applying Corollary 1 to Equation (75) with $\alpha_1 = \min(\bar{c}_1, \bar{c}_2)$, $\alpha_2 = 2^{1-\frac{\gamma_2+1}{2}} \min(\bar{c}_1, \bar{c}_2)$ and $\gamma = \gamma_2$ gives the reaching time as given in Equations (66) - (69). ■

Remark 3: Note that the virtual control signal α_2 is used to guarantee the subsystems the desired performances. However, the signal α_2 requires the derivative of the virtual control signal α_1. For simplicity in the electronics implementation of the closed loop system, the derivative is also filtered with a simple low-pass filter with a short RC time. Note that this may also incur some errors whose effects are canceled out by the incorporation of the sliding mode control at the end stage.

D. SIMULATION RESULTS

For the computer simulations of the designed controller, we take the parameter a to be $a = -0.042$, which is the value that could generate either the chaotic flow or the stable equilibriums E_1 and E_2 given in Equations (2) and (3) depending on the initial conditions, as was analyzed in Section II-B. As such, we take the initial states of the master system x_{m_0} to be:

$$x_{m_0} = [5, 1, 0.042], \tag{76}$$

which would ensure that the system generates chaotic flows. The slave system is excited with the initial states given by:

$$x_{s_0} = [1.1, 1.1, 0.042], \tag{77}$$

ensuring that the open loop system generates stable equilibrium flows. The control parameters used are:

$$c_1 = 2.4, \quad c_2 = 8.7, \quad \zeta_1 = 0.006, \tag{78}$$

$$\zeta_2 = 0.005, \quad a = 0.004, \quad \gamma_2 = 0.002, \tag{79}$$

$$D = 0.01, \quad D_1 = 0.005 \tag{80}$$

Fig.9 now shows a synchronization between the master and slave signals for x_1 - x_3 states. Fig.10 depicts the control efforts $u(t)$ needed for the synchronization. Note that the active synchronization is achieved within about 2 seconds, which is faster than the works of Vaidyanathan [43], [44], [45]. Higher c_1 and c_2 gains could of course be used to shorten the synchronization process to be well within one second, but the control efforts exuded within that one-second period will be exponentially high, and thus limited by the supply rails. This causes the actual synchronization process to be elongated to well over 2 seconds. The control efforts used in

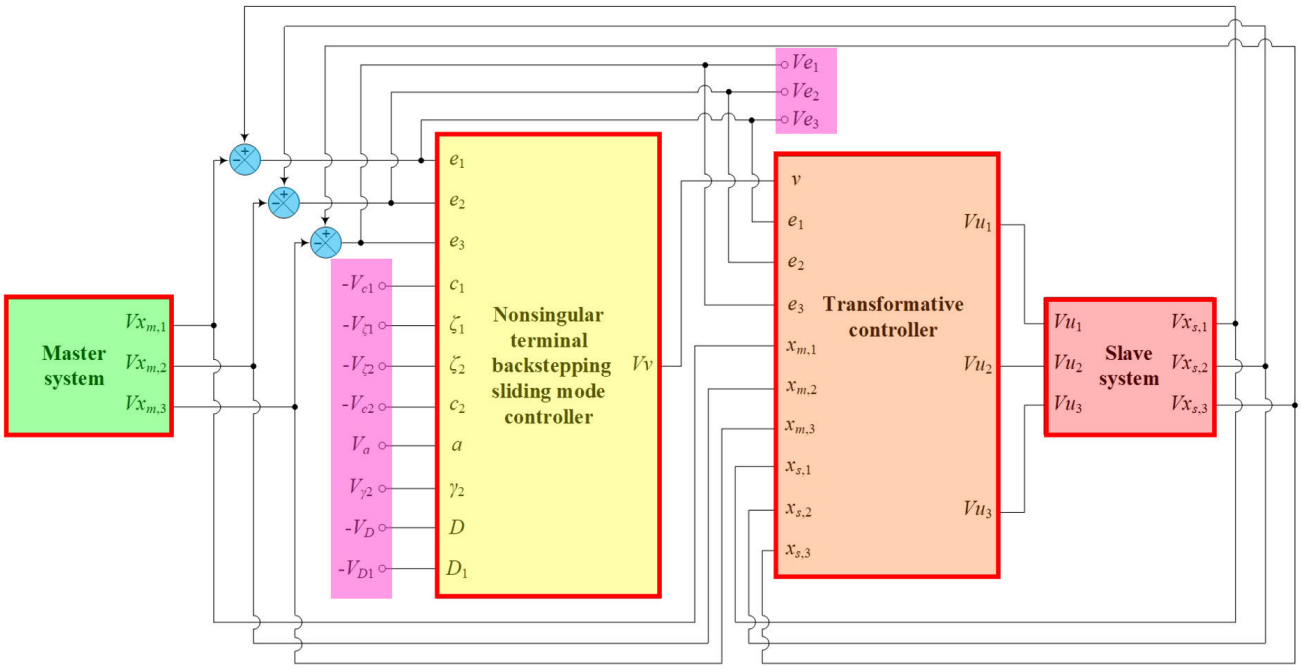

FIGURE 13. Overall schematic for the circuit implementation of the presented six-term chaotic closed-loop system.

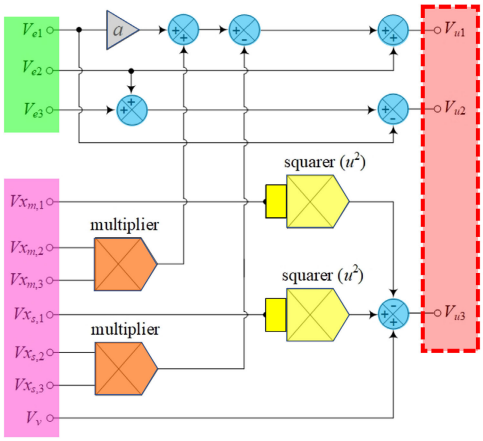

FIGURE 14. Block diagram of the transformative controller.

our case are mainly about 1200, which electronically means that for x_1 - x_3 signals in the order of mV, the main control efforts would just be around 1.2 V, which is well within the supply rails of the IC of 5 V.

The next test concerns the synchronization of chaotic systems under parameter errors and uncertainties. In this light, we consider two extreme cases. The first case is when parameter a is set to -0.084, representing a 100% decrease. The second case considered is when a is set to -0.001, which represents about 100% increase. These two cases provide the bounds for the uncertainties in parameter a, which could be anywhere in between. Fig. 11 shows the synchronization between the master and slave x_1's under these extreme parameter bounds. It is apparent from both Figs. 11a and 11b that no significant differences could be observed between the two cases as well as to the result of Fig. 9a, which was the case of the true a value. Note also that the same results are also seen with x_2 and x_3 states. The synchronization times are still similar to those of the true value case. These results imply that the designed terminal backstepping sliding mode controller is definitely robust to extreme parameter changes. This is definitely a boon for the electronics implementation, where the offset needed for the slave system does not have to be designed to be exactly a_{true}, in order to yield the same control results as the ideal case.

In order to further ascertain the presented technique, the developed controller is then compared to the normal integral backstepping sliding mode controller with the designed sliding surface given by:

$$s = \lambda_1 z_1 + \lambda_2 z_2 + \lambda_3 z_3. \tag{81}$$

with the $\lambda = [3.0, 0.3, 0.5]^T$. The switching control signal u_{sw} for this particular case is designed as:

$$u_{sw} = -D\text{signr}(s). \tag{82}$$

with D chosen as 0.01 in similar fashion to Equation (80). Note that the parameters of Equations (78) - (79) are kept unchanged. Figure 12 shows the errors e_1 - e_3 for the presented method, against the normal integral backstepping sliding mode controller. As is seen, the error system for the proposed controller converges to the origin in finite time. So we can conclude that finite time synchronization has occurred with our proposed design, and this controller achieves a good tracking performance without the chattering phenomenon.

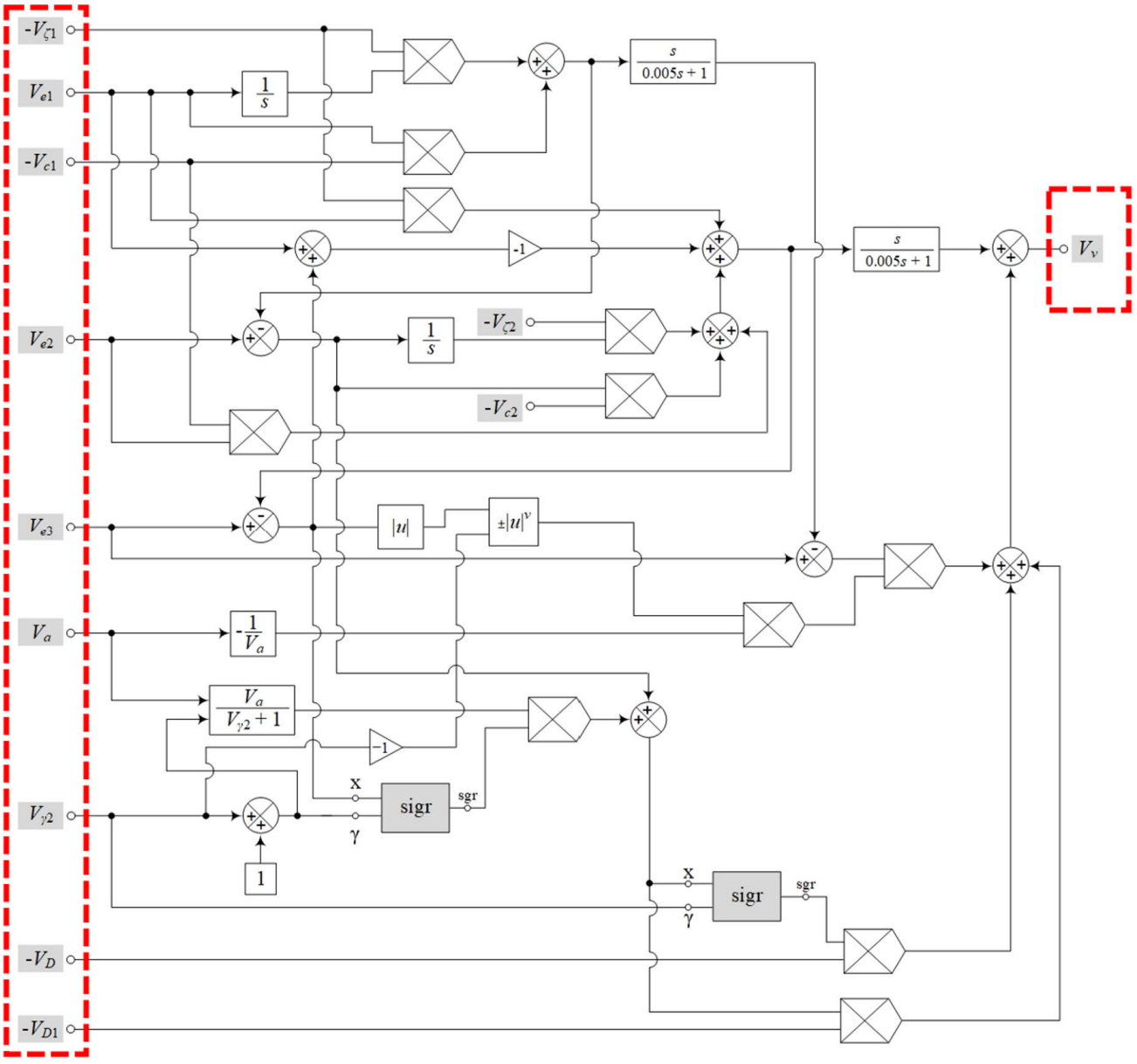

FIGURE 15. Overall schematic for the circuit implementation of the nonterminal integral backstepping sliding mode controller.

V. CIRCUIT IMPLEMENTATION OF THE CLOSED-LOOP SYSTEM

A. CIRCUIT DESIGN METHODOLOGY

The block diagram for the implementation of the presented six-term chaotic system in a closed loop is shown in Fig.13. This design comprises a master system, a nonsingular terminal backstepping sliding mode controller, a transformative controller, and a slave system. Both the master system and slave system used in this design were implemented with the open-loop system as depicted in Fig.5. The internal components of the designed controllers, a transformative controller, and a nonsingular terminal backstepping sliding mode controller, are also represented in Figs.14 - 16, respectively. The actual physical circuitry for the designed controllers has been constructed using the renowned OA-based function circuit realization [74]. Note that the descriptive equations

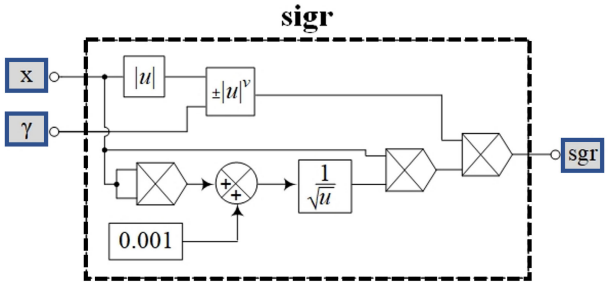

FIGURE 16. The internal detail of the `sigr` block.

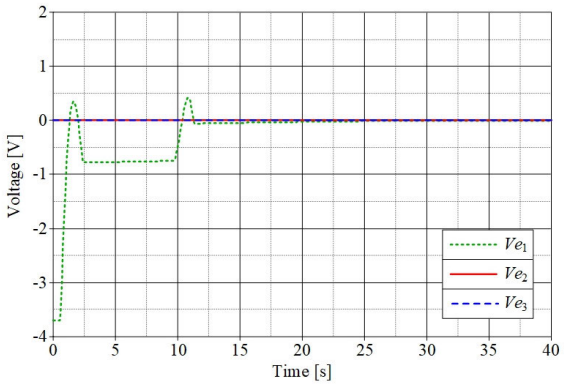

FIGURE 17. Simulated state errors of the designed system in Fig. 13.

for the master system is similar in form to Equation (19), except the variables V_{x_k} are replaced by $Vx_{m,k}$, k=1,2,3. The descriptive equations for the slave system, under the influence of the transformative controller, are designed in the spirit of Equation (22) as:

$$\dot{V_{x_{s,1}}} = aV_{x_{s,1}} + V_{x_{s,2}}V_{x_{s,3}} + V_{u_1}$$
$$\dot{V_{x_{s,2}}} = V_{x_{s,1}} - V_{x_{s,2}} + V_{u_2} \quad (83)$$
$$\dot{V_{x_{s,3}}} = 1 - V_{x_{s,1}}^2 + V_{u_3} \quad (84)$$

The transformative controller is designed based on Equations (28) - (30), whose descriptive equations are given by:

$$V_{u_1} = -aV_{e_1} - V_{x_{s,2}}V_{x_{s,3}} + V_{x_{m,2}}V_{x_{m,3}} + V_{e_2} \quad (85)$$
$$V_{u_2} = V_{e_2} - V_{e_1} + V_{e_3} \quad (86)$$
$$V_{u_3} = V_{x_{s,1}}^2 - V_{x_{m,1}}^2 + V_v \quad (87)$$

B. PSPICE SIMULATION

For simulation purposes, the initial conditions of the master system and slave system were set as Equations (76) and (77). The control parameters used in this design were: $V_{c_1} = 2.4$ V, $V_{c_2} = 8.7$ V, $V_{\zeta_1} = 0.006$ V, $V_{\zeta_2} = 0.005$ V, $V_a = 0.004$ V, $V_{\gamma_1} = 0.002$ V, $V_D = 0.01$, and $V_{D_1} = 0.005$ V, which are designed to be the same as the control parameters used in the normal simulations. The simulated state errors V_{e_1}, V_{e_2}, and V_{e_3} of the designed system are depicted in Fig.17. The results demonstrate that the master and slave signals in the presented system are well synchronized. The error signals approached 0 V in 12 seconds with the offset voltages of -45.227 mV, 6.769 mV, and -0.121 mV for V_{e_1}, V_{e_2}, and V_{e_3}, respectively. Note that the synchronization time in the analog circuitry implementation is well over the computer simulation. This is primarily attributable to the op-amp slew rates used in the circuitry implementation. Naturally, faster active devices could produce better responses, and their applications could be further studied, as could the designs of controllers with simpler topologies.

VI. CONCLUSION

In this work, a modified six-term chaotic system with only stable equilibria was first presented, whose dynamics could be changed with only one single parameter, namely a. Furthermore, this chaotic system could be transformed into other multi-wing chaotic systems through invariant transformations. Standard dynamical analysis procedures such as Lyapunov exponents and the period distribution of state variable (x_{max}) confirmed that the presented system is indeed chaotic. A basin of attraction of the system is also investigated, revealing that this system also has hidden attractors.

To synchronize this particular chaotic system, a nonlinear, nonsingular terminal integral backstepping sliding mode controller is designed. A theoretical proof is also given that provides faster-reaching bounds than the earlier works. A modification is also made to the nonsingular terminal sliding surface to accommodate the implementation of analog circuitry. Simulation results demonstrate that within 2 seconds, perfect synchronization between the master and slave systems was accomplished while remaining robust to extreme parameter uncertainties. A comparison between the finite time nonsingular terminal sliding mode controller to a normal backstepping sliding mode control revealed that the proposed controller does indeed achieve synchronization in finite time, with good tracking performances.

Finally, the six-term chaotic system is designed in circuitry through the use of commercially available op-amps (LF357) and analog multipliers (AD633), in open-loop and closed-loop configurations. In an open loop configuration, the initial values required for chaotic excitation were set through the applied voltages, whereas the system parameter is adjusted through passive components. For the closed-loop configurations, the descriptive circuitry equations are designed in such a way that mimics the actual control equations, for simplicity and ease of troubleshooting. The workability of both the open and closed-loop circuit configurations is examined through simulations in OrCAD PSpice. Results showed that the master and slave systems were found to be in synchronization with less than 0.95% maximum errors. Possible future works include the designs of nonsingular integral backstepping terminal sliding mode controllers with less complicated implementation, the incorporation of fixed time control designs such as [75] and [76], as well as the implementation of these designs using other active devices with electronic tunability such as operational transconductance amplifiers (OTAs).

ACKNOWLEDGMENT

The authors would like to thank the anonymous reviewers for their provision of valuable comments and suggestions that improved this manuscript.

REFERENCES

[1] E. N. Lorenz, "Deterministic nonperiodic flow," *J. Atmos. Sci.*, vol. 20, no. 2, pp. 130–141, Mar. 1963.

[2] Y. Miladi, M. Feki, and N. Derbel, "Stabilizing the unstable periodic orbits of a hybrid chaotic system using optimal control," *Commun. Nonlinear Sci. Numer. Simul.*, vol. 20, no. 3, pp. 1043–1056, Mar. 2015.

[3] N. Stollenwerk, L. Mateus, F. Rocha, U. Skwara, P. Ghaffari, and M. Aguiar, "Prediction and predictability in population biology: Noise and chaos," *Math. Model. Natural Phenomena*, vol. 10, no. 2, pp. 142–164, 2015.
[4] O. E. Rössler, "An equation for continuous chaos," *Phys. Lett. A*, vol. 57, no. 5, pp. 397–398, 1976.
[5] T. Matsumoto, "A chaotic attractor from Chua's circuit," *IEEE Trans. Circuits Syst. I, Reg. Papers*, vol. CSI-31, no. 12, pp. 1055–1058, Dec. 1984.
[6] J. C. Sprott, "Some simple chaotic flows," *Phys. Rev. E, Stat. Phys. Plasmas Fluids Relat. Interdiscip. Top.*, vol. 50, no. 2, pp. R647–R650, Aug. 1994.
[7] G. Van Der Schrier and L. R. M. Maas, "The diffusionless Lorenz equations; Shil'nikov bifurcations and reduction to an explicit map," *Phys. D, Nonlinear Phenomena*, vol. 141, nos. 1–2, pp. 19–36, Jul. 2000.
[8] B. Munmuangsaen and B. Srisuchinwong, "A new five-term simple chaotic attractor," *Phys. Lett. A*, vol. 373, no. 44, pp. 4038–4043, 2009.
[9] S. Jafari and J. C. Sprott, "Simple chaotic flows with a line equilibrium," *Chaos, Solitons Fractals*, vol. 57, pp. 79–84, Dec. 2013.
[10] S. Sampath, S. Vaidyanathan, C. K. Volos, and V. T. Pham, "An eight-term novel four-scroll chaotic system with cubic nonlinearity and its circuit simulation," *J. Eng. Sci. Technol. Rev.*, vol. 8, no. 2, pp. 1–6, Apr. 2015.
[11] V.-T. Pham, C. Volos, S. Jafari, Z. Wei, and X. Wang, "Constructing a novel no-equilibrium chaotic system," *Int. J. Bifurcation Chaos*, vol. 24, no. 5, 2014, Art. no. 1450073.
[12] F. Yu, C. Wang, Q. Wan, and Y. Hu, "Complete switched modified function projective synchronization of a five-term chaotic system with uncertain parameters and disturbances," *Pramana*, vol. 80, no. 2, pp. 223–235, Feb. 2013.
[13] T. Gotthans, J. C. Sprott, and J. Petržela, "Simple chaotic flow with circle and square equilibrium," *Int. J. Bifurcation Chaos*, vol. 26, no. 8, 2016, Art. no. 1650137.
[14] S. Jafari, J. C. Sprott, and M. Molaie, "A simple chaotic flow with a plane of equilibria," *Int. J. Bifurcat. Chaos.*, vol. 26, no. 6, Jun. 2016, Art. no. 1650098.
[15] J. O. Maaita, C. K. Volos, I. M. Kyprianidis, and I. N. Stouboulos, "The dynamics of a cubic nonlinear system with no equilibrium point," *J. Nonlinear Dyn.*, vol. 2015, pp. 1–13, Sep. 2015.
[16] N. V. Kuznetsov, G. A. Leonov, and V. I. Vagaitsev, "Analytical-numerical method for attractor localization of generalized Chua's system," *IFAC Proc. Volumes*, vol. 43, no. 11, pp. 29–33, 2010.
[17] G. A. Leonov and N. V. Kuznetsov, "Hidden attractors in dynamical systems: From hidden oscillations in Hilbert–Kolmogorov, Aizerman, and Kalman problems to hidden chaotic attractor in Chua circuits," *Int. J. Bifurcat. Chaos*, vol. 23, no. 1, Jan. 2013, Art. no. 1330002.
[18] M. A. Kiseleva, N. V. Kondratyeva, N. V. Kuznetsov, G. A. Leonov, and E. P. Solovyeva, "Hidden periodic oscillations in drilling system driven by induction motor," *IFAC Proc. Volumes*, vol. 47, no. 3, pp. 5872–5877, 2014.
[19] N. V. Kuznetsov, "Hidden attractors in fundamental problems and engineering models: A short survey," in *AETA 2015: Recent Advances in Electrical Engineering and Related Sciences* (Lecture Notes in Electrical Engineering), vol. 371. Berlin, Germany: Springer, 2016, pp. 13–25.
[20] J. G. Freire, C. Bonatto, C. C. DaCamara, and J. A. C. Gallas, "Multistability, phase diagrams, and intransitivity in the Lorenz-84 low-order atmospheric circulation model," *Chaos, Interdiscipl. J. Nonlinear Sci.*, vol. 18, no. 3, p. 33121, Sep. 2008.
[21] G. Datseris and A. Wagemakers, "Effortless estimation of basins of attraction," *Chaos, Interdiscipl. J. Nonlinear Sci.*, vol. 32, no. 2, Feb. 2022, Art. no. 023104.
[22] J. C. Sprott, S. Jafari, V.-T. Pham, and Z. S. Hosseini, "A chaotic system with a single unstable node," *Phys. Lett. A*, vol. 379, no. 36, pp. 2030–2036, 2015.
[23] M. Molaie, S. Jafari, J. C. Sprott, and S. M. R. H. Golpayegani, "Simple chaotic flows with one stable equilibrium," *Int. J. Bifurcation Chaos*, vol. 23, no. 11, 2013, Art. no. 1350188.
[24] L. Zhou, C. Wang, and L. Zhou, "A novel no-equilibrium hyperchaotic multi-wing system via introducing memristor," *Int. J. Circuit Theory Appl.*, vol. 46, no. 1, pp. 84–98, Mar. 2017.
[25] S. Zhang, Y. Zeng, Z. Li, M. Wang, and L. Xiong, "Generating one to four-wing hidden attractors in a novel 4D no-equilibrium chaotic system with extreme multistability," *Chaos, Interdiscipl. J. Nonlinear Sci.*, vol. 28, no. 1, Jan. 2018, Art. no. 013113.
[26] Q. Deng, C. Wang, and L. Yang, "Four-wing hidden attractors with one stable equilibrium point," *Int. J. Bifurcation Chaos*, vol. 30, no. 6, May 2020, Art. no. 2050086.
[27] Q. Xie and Y. Zeng, "Generating different types of multi-double-scroll and multi-double-wing hidden attractors," *Eur. Phys. J. Special Topics*, vol. 229, nos. 6–7, pp. 1361–1371, Mar. 2020.
[28] C. Letellier, P. Werny, J.-M. Malasoma, and R. Gilmore, "Multichannel intermittencies induced by symmetries," *Phys. Rev. E, Stat. Phys. Plasmas Fluids Relat. Interdiscip. Top.*, vol. 66, no. 3, Sep. 2002, Art. no. 036220.
[29] Y. Yang, L. Huang, J. Xiang, H. Bao, and H. Li, "Design of multi-wing 3D chaotic systems with only stable equilibria or no equilibrium point using rotation symmetry," *AEU Int. J. Electron. Commun.*, vol. 135, Jun. 2021, Art. no. 153710.
[30] M. T. Yassen, "Controlling chaos and synchronization for new chaotic system using linear feedback control," *Chaos, Solitons Fractals*, vol. 26, no. 3, pp. 913–920, 2005.
[31] F. Wang and C. Liu, "A new criterion for chaos and hyperchaos synchronization using linear feedback control," *Phys. Lett. A*, vol. 360, no. 2, pp. 274–278, Dec. 2006.
[32] M. T. Yassen, "Adaptive control and synchronization of a modified Chua's circuit system," *Appl. Math. Comput.*, vol. 135, no. 1, pp. 113–128, Feb. 2003.
[33] S. Vaidyanathan, "Adaptive chaos control and synchronization of hyper-chaotic LIU system," *Int. J. Comput. Sci., Eng. Inf. Technol.*, vol. 1, no. 2, pp. 29–40, Jun. 2011.
[34] S. Vaidyanathan, "Global chaos synchronization of the forced Van Der Pol chaotic oscillators via adaptive control method," *Int. J. Pharmtech Res.*, vol. 8, no. 6, pp. 156–166, Oct. 2015.
[35] S. Vaidyanathan, "Anti-synchronization of novel coupled Van Der Pol conservative chaotic systems via adaptive control method," *Int. J. Pharmtech Res.*, vol. 9, no. 2, pp. 106–123, Mar. 2016.
[36] A. El-Gohary, "Optimal synchronization of Rössler system with complete uncertain parameters," *Chaos, Solitons Fractals*, vol. 27, no. 2, pp. 345–355, Jan. 2006.
[37] S. Pan and F. Yin, "Optimal control of chaos with synchronization," *Int. J. Bifurcation Chaos*, vol. 7, no. 12, pp. 2855–2860, Dec. 1997.
[38] L. Huang, R. Feng, and M. Wang, "Synchronization of chaotic systems via nonlinear control," *Phys. Lett. A*, vol. 320, no. 4, pp. 271–275, Jan. 2004.
[39] H.-T. Yau and J.-J. Yan, "Chaos synchronization of different chaotic systems subjected to input nonlinearity," *Appl. Math. Comput.*, vol. 197, no. 2, pp. 775–788, Apr. 2008.
[40] H. Delavari and M. Mohadeszadeh, "Robust finite-time synchronization of non-identical fractional-order hyperchaotic systems and its application in secure communication," *IEEE/CAA J. Autom. Sinica*, vol. 6, no. 1, pp. 228–235, Jan. 2019.
[41] S. Rasappan and S. Vaidyanathan, "Hybrid synchronization of n–scroll Chua and Lur'e chaotic systems via backstepping control with novel feedback," *Arch. Control Sci.*, vol. 22, no. 3, pp. 343–365, Nov. 2012.
[42] B. A. Idowu, L. G. Dolvis, O. Guillén Fernández, A. Sambas, S. Vaidyanathan, and E. Tlelo Cuautle, "A new multistable hyperjerk dynamical system with self-excited chaotic attractor, its complete synchronisation via backstepping control, circuit simulation and FPGA implementation," *Int. J. Model., Identificat. Control*, vol. 35, no. 3, p. 177, 2020.
[43] S. Vaidyanathan, "Analysis, adaptive control and synchronization of a novel 4-D hyperchaotic hyperjerk system via backstepping control method," *Arch. Control Sci.*, vol. 26, no. 3, pp. 311–338, Sep. 2016.
[44] S. Vaidyanathan, "A new 3-D jerk chaotic system with two cubic nonlinearities and its adaptive backstepping control," *Arch. Control Sci.*, vol. 27, no. 3, pp. 409–439, Sep. 2017.
[45] S. Vaidyanathan, S. T. Kingni, A. Sambas, M. A. Mohamed, and M. Mamat, "A new chaotic jerk system with three nonlinearities and synchronization via adaptive backstepping control," *Int. J. Eng. Technol.*, vol. 7, no. 3, p. 1936, Aug. 2018.
[46] S. Rasappan and S. Vaidyanathan, "Global chaos synchronization of WINDMI and Coullet chaotic systems using adaptive backstepping control design," *Kyungpook Math. J.*, vol. 54, no. 2, pp. 293–320, Jun. 2014.
[47] S. Vaidyanathan, "Anti-synchronizing backstepping control design for Arneodo chaotic system," *Int. J. Bioinf. Biosci.*, vol. 3, no. 1, pp. 21–33, Mar. 2013.

[48] B. Vaseghi, A. M. Pourmina, and S. Mobayen, "Secure communication in wireless sensor networks based on chaos synchronization using adaptive sliding mode control," *Nonlinear Dyn.*, vol. 89, no. 3, pp. 1689–1704, Aug. 2017.
[49] I.-C. Baik, K.-H. Kim, and M.-J. Youn, "Robust nonlinear speed control of PM synchronous motor using boundary layer integral sliding mode control technique," *IEEE Trans. Control Syst. Technol.*, vol. 8, no. 1, pp. 47–54, Jan. 2000.
[50] I. Boiko and L. Fridman, "Analysis of chattering in continuous sliding-mode controllers," *IEEE Trans. Autom. Control*, vol. 50, no. 9, pp. 1442–1446, Sep. 2005.
[51] S. Mobayen, S. Mostafavi, and A. Fekih, "Non-singular fast terminal sliding mode control with disturbance observer for underactuated robotic manipulators," *IEEE Access*, vol. 8, pp. 198067–198077, 2020.
[52] T. N. Truong, A. T. Vo, and H.-J. Kang, "A backstepping global fast terminal sliding mode control for trajectory tracking control of industrial robotic manipulators," *IEEE Access*, vol. 9, pp. 31921–31931, 2021.
[53] H. Pan, G. Zhang, H. Ouyang, and L. Mei, "A novel global fast terminal sliding mode control scheme for second-order systems," *IEEE Access*, vol. 8, pp. 22758–22769, 2020.
[54] L. Qiao and W. Zhang, "Adaptive non-singular integral terminal sliding mode tracking control for autonomous underwater vehicles," *IET Control Theory Appl.*, vol. 11, no. 8, pp. 1293–1306, Feb. 2017.
[55] H. Zhang, A. Song, H. Li, and S. Shen, "Novel adaptive finite-time control of teleoperation system with time-varying delays and input saturation," *IEEE Trans. Cybern.*, vol. 51, no. 7, pp. 3724–3737, Jul. 2021.
[56] B. Chen, F. Wang, X. P. Liu, and C. Lin, "Finite-time adaptive fuzzy tracking control design for nonlinear systems," *IEEE Trans. Fuzzy Syst.*, vol. 26, no. 3, pp. 1207–1216, Jun. 2018.
[57] H. Wang, B. Chen, C. Lin, Y. Sun, and F. Wang, "Adaptive finite-time control for a class of uncertain high-order non-linear systems based on fuzzy approximation," *IET Control Theory Appl.*, vol. 11, no. 5, pp. 677–684, Mar. 2017.
[58] G. A. Leonov, N. V. Kuznetsov, and T. N. Mokaev, "Homoclinic orbits, and self-excited and hidden attractors in a Lorenz-like system describing convective fluid motion," *Eur. Phys. J. Special Topics*, vol. 224, no. 8, pp. 1421–1458, Jul. 2015.
[59] G. Datseris, "DynamicalSystems.Jl: A Julia software library for chaos and nonlinear dynamics," *J. Open Source Softw.*, vol. 3, no. 23, p. 598, Mar. 2018.
[60] G. Chen and T. Ueta, "Yet another chaotic attractor," *Int. J. Bifurcation Chaos*, vol. 9, no. 7, pp. 1465–1466, 1999.
[61] N. V. Kuznetsov, G. A. Leonov, T. N. Mokaev, A. Prasad, and M. D. Shrimali, "Finite-time Lyapunov dimension and hidden attractor of the Rabinovich system," *Nonlinear Dyn.*, vol. 92, no. 2, pp. 267–285, 2018.
[62] N. V. Kuznetsov, T. N. Mokaev, O. A. Kuznetsova, and E. V. Kudryashova, "The Lorenz system: Hidden boundary of practical stability and the Lyapunov dimension," *Nonlinear Dyn.*, vol. 102, no. 2, pp. 713–732, Aug. 2020.
[63] A. Wolf, J. B. Swift, H. L. Swinney, and J. A. Vastano, "Determining Lyapunov exponents from a time series," *Phys. D, Nonlinear Phenomena*, vol. 16, no. 3, pp. 285–317, Jul. 1985.
[64] National Semiconductor. *JFET Input Operational Amplifiers, LF357 Datasheet*, Accessed: Feb. 7, 2023. [Online]. Available: https://pdf1.alldatasheet.com/datasheet-pdf/view/97341/NSC/LF357.html
[65] Analog Devices. *Low Cost Analog Multiplier, AD633 Datasheet*. Accessed: Feb. 7, 2023. [Online]. Available: https://www.analog.com/media/en/technical-documentation/data-sheets/ad633.pdf
[66] S. Vaidyanathan, S. Jafari, V. T. Pham, A. T. Azar, and F. E. Alsaadi, "A 4-D chaotic hyperjerk system with a hidden attractor, adaptive backstepping control and circuit design," *Arch. Control Sci.*, vol. 28, no. 2, pp. 239–254, 2018.
[67] S. Vaidyanathan, A. Sambas, and S. Zhang, "A new 4-D dynamical system exhibiting chaos with a line of rest points, its synchronization and circuit model," *Arch. Control Sci.*, vol. 29, no. 3, pp. 485–506, 2019.
[68] J. Yu, P. Shi, and L. Zhao, "Finite-time command filtered backstepping control for a class of nonlinear systems," *Automatica*, vol. 92, pp. 173–180, Jun. 2018.
[69] X. Huang, W. Lin, and B. Yang, "Global finite-time stabilization of a class of uncertain nonlinear systems," *Automatica*, vol. 41, no. 5, pp. 881–888, May 2005.
[70] S. P. Bhat and D. S. Bernstein, "Finite-time stability of continuous autonomous systems," *SIAM J. Control Optim.*, vol. 38, no. 3, pp. 751–766, Jan. 2000.
[71] S. Yu, X. Yu, B. Shirinzadeh, and Z. Man, "Continuous finite-time control for robotic manipulators with terminal sliding mode," *Automatica*, vol. 41, no. 11, pp. 1957–1964, Nov. 2005.
[72] B. Deng, K. Shao, and H. Zhao, "Adaptive second order recursive terminal sliding mode control for a four-wheel independent steer-by-wire system," *IEEE Access*, vol. 8, pp. 75936–75945, 2020.
[73] Z. Xu, W. Huang, Z. Li, L. Hu, and P. Lu, "Nonlinear nonsingular fast terminal sliding mode control using deep deterministic policy gradient," *Appl. Sci.*, vol. 11, no. 10, p. 4685, May 2021.
[74] S. Franco, *Design With Operational Amplifiers and Analog Integrated Circuits*. New York, NY, USA: McGraw-Hill Education, 2015.
[75] J. Sun, J. Yi, and Z. Pu, "Fixed-time adaptive fuzzy control for uncertain nonstrict-feedback systems with time-varying constraints and input saturations," *IEEE Trans. Fuzzy Syst.*, vol. 30, no. 4, pp. 1114–1128, Apr. 2022.
[76] K. Mei, S. Ding, and C.-C. Chen, "Fixed-time stabilization for a class of output-constrained nonlinear systems," *IEEE Trans. Syst., Man, Cybern. Syst.*, vol. 52, no. 10, pp. 6498–6510, Oct. 2022.

NAPASOOL WONGVANICH (Member, IEEE) was born in Bangkok, Thailand. He received the B.E. (Hons.) and Ph.D. degrees in electrical and electronics engineering from the University of Canterbury, Christchurch, New Zealand, in 2008 and 2016, respectively.

He has been with the Department of Instrumentation and Control Engineering, School of Engineering, King Mongkut's Institute of Technology Ladkrabang (KMITL), since 2016, where he is currently an Assistant Professor. His research interests include modeling and system identification, and optimal and nonlinear control for industrial electronics, robotics, and biomedical applications.

Dr. Wongvanich is serving as a Treasurer for the IEEE Control Systems Society Thailand.

NATCHANAI ROONGMUANPHA received the B.Eng. degree in electronics engineering and the M.Eng. degree in control engineering from the School of Engineering, King Mongkut's Institute of Technology Ladkrabang (KMITL), Bangkok, Thailand, in 2016 and 2019, respectively, where he is currently pursuing the Ph.D. degree in electrical engineering. During his master's degree, he has created several adjustable inductance simulator circuits, which resulted in conference presentations and published papers. He is currently a Lecturer with KOSEN-KMITL. His current research interests include immittance function simulators and active analog filter design.

WORAPONG TANGSRIRAT received the B.Ind.Tech. degree (Hons.) in electronics engineering and the M.Eng. and D.Eng. degrees in electrical engineering from the Faculty of Engineering, King Mongkut's Institute of Technology Ladkrabang (KMITL), Bangkok, Thailand, in 1991, 1997, and 2003, respectively. Since 1995, he has been a Faculty Member with KMITL, where he is currently a Full Professor in electrical engineering with the Department of Instrumentation and Control Engineering. He has edited or written 15 books, and has more than 100 research articles published in peer-reviewed international journals. His research interests include analog signal processing and integrated circuits, current-mode circuits, active filter and oscillator design, and electronic instrumentation and control systems. He is named in the list of the "Top 2% of Scientists in the World," reported by Stanford University.